NASA CR-145001

PARAMETRIC STUDY OF THE NOISE PRODUCED BY THE INTERACTION OF THE MAIN ROTOR WAKE WITH THE TAIL ROTOR

by

John C. Balcerak

Prepared under Contract NAS1-13690

by

RASA Division
Systems Research Laboratories, Inc.
Newport News, Virginia 23602

for

NATIONAL AERONAUTICS AND SPACE ADMINISTRATION

FOREWORD

The overall research described in this report was conducted by the RASA Division of Systems Research Laboratories, Inc. in Rochester, New York under the management of Mr. Richard P. White, Jr. The model was designed and fabricated by the Aerosystems Research Division in Dayton, Ohio, under the management of Dr. Karlheinz O. W. Ball.

The Contract Technical Manager for the program was Mr. Robert J. Pegg, Noise Control Branch, NASA/Langley.

TABLE OF CONTENTS

PARAMETRIC STUDY OF THE NOISE PRODUCED BY THE INTERACTION OF THE MAIN ROTOR WAKE WITH THE TAIL ROTOR*

By John C. Balcerak
RASA Division, Systems Research Laboratories, Inc.

ABSTRACT

A model was designed, fabricated and wind tunnel tested to identify some of the parameters which were pertinent to the noise produced by the interaction of the main rotor wake with the tail rotor. The model provided for variations in many geometric and operating parameters.

The initial set of tests indicated that the noise produced by the tail rotor was, in general, sensitive to the location of the vortex interaction on the tail rotor disk, direction of rotation, lateral rotor-fin spacing, tip speed and the operating mode of the tail rotor; and generally insensitive to main rotor thrust coefficient, longitudinal spacing and tail rotor-to-main rotor rotational speed ratios. The noise produced by changes in some of the parameters were more sensitive to changes in advance ratio than others.

Theoretical analyses, using a simplified aerodynamic representation of the interaction phenomenon in conjunction with an existing noise prediction theory, showed good qualitative correlation in predicting the trends shown by the experimental data. Quantitative correlation was inappropriate because of the simplifications in the representation. Refinements in the analyses to adequately predict the noise phenomenon have been outlined to complement further experimental investigations.

INTRODUCTION

One of the major sources of noise produced by a helicopter, is that produced by the tail rotor. This noise is generally characterized by a directivity in which the maximum intensity of the noise occurs along the flight path of the helicopter. To a large extent, the intensity of this noise is affected by the interaction of the tail rotor blades with the wake of the main rotor, or more specifically, with its tip vortex(es). The tail rotor can intersect the tip vortexes that are trailed off the aft portion of the main rotor disk near $\psi = 0$, and those that are tailed off the forward portion of the disk near $\psi = 180°$. These intersections can occur singly or in tandem. Further, there may be tandem intersections by the vortexes that are trailed off the main rotor at the same azimuthal location at successive revolutions of the main rotor.

*The contract research effort which has lead to the results in this report was financially supported by USAAMRDL (Langley Directorate).

It is obvious that many parameters can affect the noise characteristics that are produced by the noted interactions. Geometrically, the longitudinal, lateral and vertical spacings of the tail rotor relative to the disk plane of the main rotor enter into the problem, as these spacings affect the points of the intersection of the main rotor wake. The flight parameters are also significant, as the wake geometry is a function of the trim variables, which vary with advance ratio, as well as the main rotor disk loading which determines tip vortex strength. Other parameters, such as the rotor tip speeds, the tail rotor operating mode-tractor vs pusher, the fin blockage, the direction of rotation also affect the interaction noise characteristics.

Analytically, the interaction problem is a little more difficult to represent than say, interactions of the main rotor with its own wake. This is so since the ratio of tail rotor-to-main rotor speed is seldom an integer, so that the problem is nonperiodic. Simplifications in the representation of the non-periodicity are possible, but even with this aspect, comparatively little effort has been expended to date to predict and analyze the noise produced by the interaction of a rotor with its own or another wake.

In view of the complexity of the problem and the lack of suitable analysis techniques to study the problem in detail, an experimental program was conducted in order to further the understanding of this noise phenomenon. Interest in the experimental approach to the problem was also spurred by the fabrication of an anechoic test facility at NASA/Langley in which tests could be conducted to study this and other noise phenomena. Although wind tunnel tests were not conducted in this facility, the model which was fabricated for the test program was designed to be compatible with the NASA facility.

The program thus had several objectives. The overall objective of the program was to determine whether main rotor wake/tail rotor interaction noise is or can be significant. objectives was the design and fabrication of a model which would eventually be used as a tool for investigating main rotor wake/tail rotor interaction noise phenomena in the NASA anechoic test facility. Another objective was to obtain a set of data which would identify the parameters which were most pertinent to the interaction noise problem. The third specific objective was to utilize an existing theory to represent the aerodynamic environment in the interaction phenomena, to correlate some of the experimental and theoretical results, and to determine whether refinements in the theory would be necessary or desirable in order to predict the pertinent noise characteristics adequately. These objectives of the program were achieved as described in the succeeding discussion.

LIST OF SYMBOLS

C_T	thrust coefficient
C_Q	torque coefficient
ℓ_x	longitudinal spacing between main rotor disk and tail rotor disk, cm
ℓ_y	lateral spacing between longitudinal centerline of helicopter and tail rotor disk plane, positive to right, cm
R	blade radius, cm
V	velocity, m/sec
α_s	shaft tilt angle, deg
α_z	tail boom tilt angle, deg
β_o, β_{1c}, β_{1s}	flapping coefficients; $\beta = \beta_o - \beta_{1c} \cos \psi - \beta_{1s} \sin \psi$
θ_o	collective pitch angle, deg
μ	advance ratio
ψ	azimuthal position of main rotor blade, deg
Ω	rotational speed, rpm

ABBREVIATIONS

cm	centimeters
m	meters
N	newtons
MR	main rotor
TR	tail rotor

DESCRIPTION OF MODEL AND INSTRUMENTATION

A. Model

The model used for the test program was designed to approximately a 1/16th scaled version of a UH-1 series helicopter. Figure 1 is a schematic diagram of the model. The main rotor blades were 0.914m in diameter, 4.445cm in chord and had a twist of -8° from the blade root to blade tip. The airfoil section was an NACA 0015. The blades were hinged at the 0.042 radius of the blade. Two sets of tail rotor blades were used in the test program. The first set was of the approximate 1/16th scale, and had a 0.1905m diameter and a 1.143cm chord. The second set of blades was 0.254m in diameter with a 1.143cm chord. Both sets of blades had an NACA 0015 airfoil section, were untwisted and were mounted as cantilever beams to the tail rotor hub. The standard directions of rotation of the main and tail rotors are shown in Figure 2. For the main rotor, the standard direction of rotation was such that the rotational vector was upward; for the tail rotor the rotational vector was to the left when looking upstream. The standard tip mach numbers of the main and tail rotors were the same, at $M \doteq 0.3$.

The model provided capability for variations in many main rotor wake/tail rotor interaction parameters. Table I below lists these parameters, their range of variability and the readout system for each parameter.

The change in the collective pitch settings of the main and tail rotor blades was facilitated by jigs which were bolted to the hub assembly of each rotor. Micrometers, which were an integral part of the jig were preset, and the blades were then pitched manually so that protruding pins at the blade root contacted the micrometer head. The blades were then friction-clamped to the split-hub assembly. The other manual readouts of model parameters were those for lateral spacing of the tail rotor plane with respect to the centerline of the fuselage, which was simply read by a scale, and the shaft tilt, which was read by means of a built-in vernier protractor. Calibrations of the electrical readout systems for the other parameters are given in Reference 1.

The thrust of the main and tail rotors was measured by load cells. Three 44N cells were installed around the periphery of the main rotor drive shaft to monitor the thrust of the main rotor. The thrust of the tail rotor was reacted by a 222N load cell which was installed within the fuselage at the base of the tail boom. The thrust of the tail rotor was thus calculated using the distance from the center of the hub to the center of the load cell as the moment arm. The output signals of all load cells were read on digital voltmeters.

B. Model Proof Tests

The geometric parameters listed in Table I were determined during initial calibration tests. Since the vertical spacing of

TABLE I ADJUSTABLE MODEL PARAMETERS

Parameter	Range	Readout System
Main Rotor Collective Pitch Angle	0 - 20° (1)	Micrometer
Tail Rotor Collective Pitch Angle	0 - 8° (1)	Micrometer
Tail Rotor Lateral Spacing	±1.85cm to ±2.97cm	Scale
Shaft Tilt Angle	0 to -15°	Vernier Protractor
Tail Rotor Longitudinal Spacing	2.20cm to 18cm (2)	Digital Voltmeter
Tail Rotor Vertical Spacing (3)	-19° to +12°	Digital Voltmeter
Main Rotor Rotational Speed	0 to 4100 RPM (4)	Frequency Counter
Tail Rotor Rotational Speed	0 to 13,000 RPM	Frequency Counter
Tail Rotor Direction of Rotation	-	Visual

(1) Maximum Practical Range

(2) The maximum spacing is 15.0cm for the 0.254m diameter tail rotor.

(3) The vertical spacing is provided by pitching the tail boom.

(4) Higher rotational speeds are possible at lower collective pitch angles than tested in this program.

the tail rotor was effected by pitching, there was a fore-and-aft displacement of the tail rotor as it was pitched. This displacement can be accounted for appropriately, and these details are also described in Reference 1.

In addition to the checkout of the geometric parameters, the model was proof tested to 20 percent above its nominal design parameters in relation to main rotor and tail rotor rotational speeds and main rotor and tail rotor thrust. During wind tunnel testing, the model was proof tested to 20 percent over the maximum specified forward test velocity. Appendix A lists the conditions at which the tests were conducted, and Reference 1 contains the data derived from the various calibration tests that were conducted.

C. Acoustic Instrumentation

Six microphones were used in the test program. All were B&K Type 4133 free-field microphones. The acoustic signals were amplified by Ithaco Model 453 Amplifiers, and recorded on an Ampex Model FR1300 FM Tape Recorder. The acoustic signals were also paralleled to a UA500 Ubiquitous Spectrum Analyzer. The spectra were plotted on a BBN 715 Plotamatic plotter. The microphones were calibrated frequently at various intervals throughout the test program by means of a GR1557-A Calibrator, which produced a signal of 124 dB at 250 Hz. The frequency range for the microphones was from 5 Hz to 12.5 kHz, while the response of the tape recording system was flat within ± 3 dB to 20 kHz. Overall noise levels were monitored on a B&K Type 2203 Sound Level Meter. These noise levels were recorded from visual readout of the dial indicator on the meter.

In addition to the acoustic signals, the output signals of the main and tail rotor rotational speed sensors were also tape recorded, as well as the signals from an IRIG B time-code generator. The tape records were also identified by using one channel for a voice track. A BBN Model 501 accelerometer was also mounted on the upper part of the model pylon, and the output signals from this sensor were also tape recorded. The accelerometer data were monitored during preliminary tests to determine and hence to isolate the model support assembly from rotational speeds at which resonances occurred. Although the data were tape recorded, the data were not further analyzed in detail.

The tape records were taken at 30 ips (54 kHz center frequency).

WIND TUNNEL TESTS

The wind tunnel tests were conducted in the Bolt Beranek and Newman High-Speed Anechoic Wind Tunnel. A description of this facility is given in Reference 2.

A schematic diagram of the installation which also shows the positions of the microphones, is shown as Figure 2, and a photograph of the model as installed in the wind tunnel is shown in Figure 3. The wind tunnel tests were conducted in hover and at speeds of 9.1, 20.1 and 28.4 m/sec, which corresponded to advance ratios of 0.09, 0.20 and 0.28 at the nominal main-rotor rotational speed of 2120 rpm. Background noise levels at V = 0 and at the three forward speeds for one microphone are given in Appendix B. These noise levels were obtained with the main and tail rotor blades removed from the model, but with the main-rotor motor drive running at its nominal speed (2120 rpm). The dominant characteristic of the background noise was a low frequency peak, which is believed to be associated with the impingement of the jet on the collector at the exhaust end of the chamber. The low frequency noise peaks at $\nu = 0$. The main rotor motor drive noise was below the ambient noise at all microphone positions. As the tail rotor blade passage frequency was 360 Hz, the low frequency background noise levels had little effect on the measured data, and the measured data were well above the background noise levels in the frequency range of interest, 0 to 5 kHz. As shown in Figure 3, the microphones were positioned out of the shear layer of the flow and no corrections were applied to the measured data.

A set of model parameters was defined as a reference configuration for the wind tunnel tests. Tests were conducted for this configuration and then for configurations in which only one parameter was varied from the defined set. Table II lists the test parameters for the reference configuration and the pertinent variation that was made for each other configuration that was tested. As the vertical spacing of the tail rotor was remotely controllable, data were collected for at least three vertical spacings of the tail rotor for each configuration at each advance ratio tested, except for hover. A listing of the test conditions for all configurations is given in Appendix A.

The load cells for measuring the main rotor thrust and the torque due to the tail rotor thrust were calibrated during the model proof tests. Measurements of the main rotor thrust and tail rotor torque in hover were also made with the model installed in the wind tunnel. The measurements of the main rotor thrust, which was reacted by three load cells, were inconsistent, but were near the values predicted by the D0865 NASA trim analysis. The measurements of the tail rotor thrust were consistent, although the sensitivity of the output of the load cell was somewhat less than desirable. There was also a variation in the output voltage of the torque load cell with the vertical position of the tail rotor. In spite of these difficulties, the model was set in approximate trim in hover and at advance ratios of 0.09, 0.20 and 0.28. During the tests at $\mu > 0$ it was noted that large 2/rev and 4/rev loads were being imposed on the main-rotor load cells, and further aggravated the readout of the steady load signals. From the measured data and the calculated trim conditons, however, the parameters listed in Table III were used to set the various configurations in trim.

TABLE II DESCRIPTION OF MODEL PARAMETERS COMPRISING THE TEST CONFIGURATIONS

Configuration No.	Model Parameters
1	Main Rotor: R_{MR} = 45.72cm Ω_{MR} = 2120 rpm $C_T \simeq 0.005$ Tail Rotor: R_{TR} = 0.52cm Ω_{TR} = 10800 rpm ℓ_y = -1.90cm (Tractor) ℓ_x = 2.20cm Rotational Vector to Left Fin Blockage Area: 25% of Disk Area
The parameters for the following configurations are the same as those for Configuration 1 except as noted below.	
2	ℓ_x = 14.90cm
3	ℓ_y = -2.86cm
4	Fin Blockage Area: 12% of Tail Rotor Disk Area
5	ℓ_y = +1.90cm (Pusher)
6	Tail Rotor Rotational Vector to Right
7	R_T = 12.7cm; (Tail Rotor positioned farther aft, but ℓ_x = 2.20cm
8-1	Ω_{TR} = 9720 rpm
8-2	Ω_{TR} = 10600 rpm
9	$C_T \simeq 0.007$

TABLE III MODEL PARAMETERS FOR TEST CONFIGURATIONS

MAIN ROTOR							
	Measured			Calculated			
Configuration	Advance Ratio	Collective Pitch Angle, deg	Shaft Tilt, deg	C_{T_3} x10	β_o	β_{1c}	β_{1s}
1,2,3,4,	0	14	0	5.28	0.74	-	-
5,6,7,	0.09	12	- 3.0	4.80	0.64	0.94	0.05
8-1,8-2	0.20	12	- 6.0	4.64	0.60	2.15	0.15
	0.28	14	-10.0	5.23	0.70	3.79	0.27
9	0	16	0	7.36	1.07	-	-
	0.09	14	- 3.0	6.78	0.94	1.36	0.09
	0.20	14	- 6.0	7.06	0.97	3.06	0.24
	0.28	16	-10.0	7.92	1.11	5.18	0.46

TAIL ROTOR			
	Measured		
Configuration	Advance Ratio	Collective Pitch Angle, deg	C_{Q_3} x10
1,3,5,6	0	6.0	0.255
	0.09,0.20,0.28	4.0	0.171
2	0.09,0.20,0.28	3.0	0.156
4	0	6.0	0.356
	0.09,0.20,0.28	4.0	0.238
7	0,0.09,0.20,0.28	2.0	0.174
8-1	0,0.09,0.20,0.28	4.6	0.177
8-2	0	5.9	0.239
	0.09,0.20,0.28	4.0	0.162
9	0	7.0	0.298
	0.09,0.20,0.28	5.0	0.212

The settings of the main rotor collective pitch angles were selected to duplicate the trend of collective pitch angle with advance ratio. Therefore, for the main rotor, only two sets of collective pitch settings were required for any particular configuration. One set was used for hover and at an advance ratio of 0.28, while another set was used at advance ratios of 0.09 and 0.20. Only two collective pitch settings were used for the tail rotor for any particular configuration. One setting was used for hover, while another set was used for advance ratios of 0.09, 0.20 and 0.28. An average value of the tail rotor collective pitch setting was used at $\mu \geq 0$, as it was assumed that the fin provided some of the anti-torque requirement.

The parameters listed in Table III refer to the acoustic data recorded from Record Nos. 55 through 189, which are discussed in the body of this report. Some preliminary data were taken at slightly different trim parameters and microphone positions (Record Nos. 1 through 54). These data are listed in Appendix A.

Flow visualization tests were undertaken using the internal smoke system. The smoke system functioned well during its checkout, but difficulties were encountered subsequently with the heater unit, and precluded photographic documentation of the main rotor wake/tail rotor interactions. The visual and limited photographic documentation that was obtained during checkout, however, indicates that sufficient smoke can be adequately entrained in the tip vortices for photographic documentation. Thus, the installed system should be very useful for future investigations conducted with the model.

DISCUSSION AND EVALUATION OF RESULTS

As noted in appendix B, data was obtained for approximately 170 test points (excluding calibrations) during the test program. For each of these test points noise data were recorded and spectrum analyzed for the acoustic signals from six microphones. The spectra that are presented in this report and discussion that follows is thus necessarily concentrated on the salient features that were noted from the analysis of this volume of data. In order to effect a measure of conciseness with a measure of completeness in the discussion and the figures, much of the data shown in the figures is given for only one microphone position. The position selected (Microphone 4) appeared to exemplify the typical changes in the noise characteristics for the various parametric changes. In addition, some constraint had to be exercised in relation to the number of figures showing the effects of vertical tail-rotor positioning. Pertinent data relating to other microphones or various tail-rotor positions, however, have been included. In spite of these constraints, it is believed that the ensuing discussion and figures reflect the substantive results of the program in their totality. The measured pressure time histories were analyzed from strip-chart records. The pressure peaks which may have been attributed to main rotor wake/tail rotor interactions were, however, often obscured by main rotor noise peaks. Further, because of the non-periodicity of the interaction phenomena, more exhaustive analyses of these data would be required to establish the interaction peaks more definitively, and these data are not presented herein.

As the tests were constrained to wind tunnel speeds of approximately 30 m/sec, and as the advance ratio was one of the parameters to be investigated, the rotor tip speeds were constrained to be on the order of 100 m/sec. With this tip speed, however, the effects of compressibility were eliminated as a parameter. Along with the elimination of compressibility as a parameter, it would be expected that the noise produced by main rotor wake/tail rotor interaction might not have all the characteristics that it does for full-scale helicopters. For example, if the magnitude of the noise generated by the interaction is caused by the tail rotor blade entering the drag divergence regime because of the superposition of the induced velocity of the vortex on the blade, the interaction peaks would not have the same relative significance in the model results due to the much lower tip speeds.

Also, the interaction phenomenon of the main rotor wake with the tail rotor is nonperiodic, unlike the phenomenon of the interaction of a rotor with its own wake. This nonperiodicity manifests itself in noise spectra by peaks which are associated with multiples of either the sum or difference of the tail rotor and main rotor rotational speeds. In high tip speed rotors, and in certain flight conditions, the noise levels of these peaks can be well above those of either the main or tail rotor harmonics, particularly at higher harmonics. In the model rotor, partially because of its lower tip speeds, it would also be expected that these peaks would be somewhat more prevalent at lower harmonic orders.

In analyzing data, a question always arises as to the accuracy and repeatability of the data. As regards the present data, it might be asked what changes in sound pressure levels would indicate whether a pertinent parameter effected changes in the noise produced by main rotor wake/tail rotor interaction. A measure of the repeatability and accuracy of the noise data was obtained in the test program by comparison of the data for the same configuration at different times in the test program. Configuration 1, for example, was tested both early and late in the test program. Comparison of the spectra for comparable test conditions showed that the spectra were most consistently repeatable at an advance ratio of 0.09. In this case, the noise levels of the tail rotor harmonics showed a difference of 2 dB or less in the frequency range from 0 to 5 kHz. At $\mu = 0.20$ and 0.28, similar results were also obtained, but one or two isolated harmonics showed differences of up to 4 dB. As will be noted in some of the ensuing discussion, some changes in test parameters also effected such a change in the spectrum on occasion for reasons which could not be explained. On the basis of these data, it is believed that the spectra would be repeatable within ± 2 dB, and that differences of greater than say, 5 dB in the sound pressure levels between configurations would be considered to be of primary interest in the analyses.

The bandwidth of all spectra presented in the report was 10 Hz. Although overall sound levels were also monitored and recorded, little useful information could be derived from these data as the rather high noise level of the low-frequency peak of the background noise tended to dominate the data. For sake of completeness, however, the measured overall noise data are listed in Appendix C.

A. Configuration 1 - Reference Configuration

The noise spectra at V = 0 at one microphone location for the reference configuration are shown in Figures 4, 5 and 6. Figure 4 is the spectrum of the main rotor with the tail rotor at Ω = 0. The first few harmonics of the main rotor blade passage frequency (70.7 Hz) are about 10 - 15 dB above the rest of the harmonics up to a frequency of approximately 1000 Hz. Above 1000 Hz the noise levels drop gradually about another 10 dB from about 65 dB @ 1000 Hz to about 55 dB at 5000 Hz. Figure 5 is the spectrum of the tail rotor with the main rotor at Ω = 0. Thirteen harmonics of the tail rotor blade passage rotational noise are clearly distinguishable and the absolute noise levels are about 5 - 10 dB higher than those of the main rotor up to about the 10th harmonic of the blade passage frequency. The spectrum also shows noise peaks at the tail rotor blade rotational frequency, which are believed to stem from some small asymmetry in the tail rotor blades. The hover spectrum, with both rotors at their nominal rotational speed, is shown in Figure 6, and as might be expected from the data shown in Figures 4 and 5, the spectrum appears to be a superposition of the noise of each rotor in the absence of the other except for the third harmonic which showed a drop of 10 dB which cannot be explained on a logical basis. The spectra at ν = 0 for this and other configurations were also characterized by intermittent spurious peaks near 100 Hz. The precise reason for the appearance of these peaks was not found as less emphasis was placed on this phenomenon since the peaks only occurred at a frequency which was well below the tail rotor blade passage frequency.

The noise spectra for two microphone positions, at an advance ratio of 0.09 are shown in Figures 7 and 8. In the first case (Figure 7), the tail rotor was near its full-down position so that the main rotor wake which was trailed off near ψ = 0 intersected the tail rotor disk on the upper or advancing side. The noise levels of the spectrum, except for a few harmonics, are generally lower than those in hover, particularly at some of the lower harmonics of the tail rotor blade passage frequency. The harmonics above the fourth, however, are very distinct as they were in hover at Microphone 4 and less distinct at Microphone 2. This characteristic is probably due to the directivity of the noise.

Figure 8 shows the noise spectra for the same conditions as noted in Figure 7, except that the tail rotor was near its full-up position, so that MR/TR interactions would occur on the lower or retreating side of the tail rotor disk. These data, exhibited some additional peaks near the harmonics from the 3rd through the 7th of the tail rotor blade passage frequency, which were not present when the main rotor wake intersected the tail rotor disk on the upper or advancing side of the disk. These peaks occur at a frequency corresponding to the difference between the tail and main rotor frequencies. This type of phenomenon would be expected for

a blade vortex interaction on the retreating side of the tail rotor disk. Also, the fourth harmonic, which was somewhat obscured in the spectra shown in Figure 7, became distinct in the spectra shown in Figure 8.

The noise spectra for two microphone positions at an advance ratio of 0.20 are shown in Figures 9 and 10. In the first case, (Figure 9) the tail rotor was near its full down position. In this position, calculations* show that the main rotor wake that was trailed off near $\psi = 0$ intersected the disk plane of the tail rotor near the top of the disk. For Microphone 4, there was a maximum increase of about 8 dB in the sound pressure levels of some harmonics from those measured at $\mu = 0.09$ at the same vertical position of the tail-rotor, however. It is not believed that this difference stems solely from the increase in forward velocity or from the point of intersection of the main rotor wake with the tail rotor, as the calculations also showed that the main rotor wake that was trailed off near $\psi = 180°$ also interacted with the tail rotor. Further, the point of interaction was shown to be only slightly below that of the wake that was trailed off near $\psi = 0$. This condition would be more likely to increase the noise levels than the change in forward velocity or the calculated change in the point of interaction of the isolated vortex. The spectra at $\mu = 0.20$ for the tail rotor in the down position, are also characterized by many intermediate peaks between the peaks of the tail rotor harmonics. These peaks were believed to be more associated with the noise produced by the tail rotor operating in the overall turbulent wake of the main rotor, rather than with interaction with its tip vortexes, per se.

When the tail rotor was near its full-up position, interactions would occur on the lower or retreating side of the disk. The spectra do not change significantly from those of Figure 9 with regard to the absolute noise levels of the tail-rotor harmonics. Peaks are also exhibited near the tail rotor harmonics from the 3rd through the 7th. The frequency associated with these peaks corresponds to the difference of the tail and main rotor frequencies. The peaks are somewhat obscured by the shift in the scale of the plot from that at $\mu = 0.09$ (Figure 8), but the noise levels of these peaks relative to the respective harmonics are about the same.

The noise spectra for two microphone positions at an advance ratio of 0.28 are shown in Figures 11 and 12. The spectrum in Figure 11 is for the tail rotor near its full-down position. In this case, the spectra are not drastically changed from those at $\mu = 0.20$. This condition might be expected since the position of the main rotor wake would not be expected to change appreciably between $\mu = 0.20$ and $\mu = 0.28$. A different result is shown in Figure 12, however, where the tail rotor was near its full-up position, in that the spectra for $\mu = 0.28$ do not show peaks associated with the difference of the tail and main rotor frequencies, as they did at $\mu = 0.09$ and 0.20. This result indicates the sufficient changes in wake geometry have been effected by the change in advance ratio so as to eliminate the interaction peaks.

* see Section J for detailed discussion

The characteristic geometry of the main rotor wake as a function of the advance ratio in relation to the vertical position of the tail rotor was noted to have a notable effect on the noise produced by the tail rotor. In its down position, the noise produced by the tail rotor generally appeared to be more affected by the overall main rotor wake turbulence rather than by main rotor tip vortex/tail rotor interaction. In its up position, interaction peaks, characteristic of blade/vortex interaction, were exhibited in the noise spectra at $\mu = 0.09$ and 0.20, but not at $\mu = 0.28$. This result was a little surprising, as it would be expected that there would be more of a difference in the wake geometry between $\mu = 0.09$ and $\mu = 0.20$, than between $\mu = 0.20$ and $\mu = 0.28$.

B. Configuration 2 - Effect of Change in Longitudinal Spacing

A noise spectrum for this configuration at an advance ratio of 0.20 with the tail rotor in its full-down position is shown as Figure 13. The comparable record for the reference configuration is shown in Figure 9. There are only slight differences between these spectra and a similar result was noted in comparison of the spectra at other microphone positions and advance ratios. The slight differences in the spectra are not surprising as the tip vortexes from the main rotor would be expected to intersect the tail rotor at about the same locations on the tail rotor disk for comparable vertical tail rotor positions. The collective pitch angle of the tail rotor for this configuration was reduced to 3° from its value of 4° for the reference configuration, so as to maintain the anti-torque moment about the same. As noted, however, this change in the disk loading effected almost no change in the noise spectrum. Similar results were also noted in the comparison of the noise spectra between this and the reference configuration for other vertical positions of the tail rotor. On the basis of the noted results, it was concluded that the longitudinal spacing between the disks of the main and tail rotors was not a primary parameter with regard to the pertinent noise phenomenon.

C. Configuration 3 - Effect of Change in Lateral Spacing

Noise spectra for this configuration for the full-down position of the tail rotor at advance ratios of 0.09, 0.20 and 0.28 are shown in Figures 14, 15 and 16, respectively. There was an increase of about 10 dB in the sound pressure levels of the first three harmonics of the tail rotor speed from those at $\mu = 0.09$ to those at $\mu = 0.20$ or $\mu = 0.28$. This increase was about 3 to 5 dB higher than was noted for the reference configuration. Also in going from an advance ratio of 0.20 to an advance ratio of 0.28, there was an increase in the sound pressure levels of the 5th, 6th and 7th harmonics which was a little more pronounced than it was for the reference configuration.

With respect to the reference configuration, however, at $\mu = 0.09$, there was up to a 10 dB drop in the sound pressure levels when the tail rotor was shifted to the left with respect to the fin about 0.1 of the tail rotor radius. A similar decrease in the sound pressure levels was also noted at $\mu = 0.20$ and at $\mu = 0.28$, but the drop at $\mu = 0.20$ was not as pronounced as it was at $\mu = 0.09$ except for some of the higher harmonics. Similar results were noted in the analysis of the spectra of Microphones 1, 2, 3 and 5. The reason for the noted phenomenon is believed to be associated with the proximity of the tail rotor to the fin, insofar as the fin may affect the flow upstream of the tail rotor and the flow of the main rotor wake through the disk plane of the tail rotor to a large extent. On the basis of these results, it is believed that decrease in tail rotor noise may be effected by prudent selection of the spacing between the fin and the tail rotor disk plane.

D. Configuration 4 - Effect of Change in Fin Blockage Area

Noise spectra for this configuration for the full-down position of the tail rotor in hover and at an advance ratio of 0.20 are shown in Figures 17 and 18, respectively. For the reference configuration, the fin blocks off 25 percent of the tail-rotor disk area, while for this configuration, the blockage area is 13 percent. The collective pitch angles of this configuration were maintained the same as those of the reference configuration although there was some measurable difference in the tail rotor thrust between the fin-on and fin-off configuration.

The hover spectrum for this configuration appears to differ from that of the reference configuration only in the magnitude of the sound pressure levels of the 3rd through 6th harmonics, the 3rd and 4th being about 5 dB higher than the reference configuration and the 5th and 6th being about 5 dB lower. Since there are no interaction effects in hover, this result is attributed to the peculiarities associated with blockage effects.

At an advance ratio of 0.20, the sound pressure levels decrease with increasing harmonic number from the 1st through the 7th harmonic except for the fifth. The fifth is quite dominant but the noted characteristic behavior and the drop in the sound pressure levels above the 5th harmonic indicates that the change in fin blockage had probably affected the wake flow to a large extent in the proximity of the tail rotor. This characteristic was not noted at an advance ratio of 0.28, however, and the sound pressure levels at $\mu = 0.09$ were generally above those of the reference configuration. The spectra at other microphone positions showed the same type of inconsistent characteristics. On the basis of these data, no conclusive results could be established relative to the effects of fin blockage in the interaction noise phenomenon, particularly as related to the effects of advance ratio.

E. Configuration 5 - Effect of Change in Tail Rotor Mode

The tail-rotor mode of the reference configuration was defined to be a tractor, that is, the flow blockage in its positioning occurred on the downwash side of the rotor. The mode of the pusher (Configuration 5) was such that the flow blockage occurred on the inflow side of the rotor. The lateral offset of the tail rotor from the longitudinal centerline of the helicopter, and its collective pitch schedule with advance ratio were the same as the reference configuration. Noise spectra for this configuration in hover and at advance ratios of 0.09, 0.20 and 0.28 for the full-down position of the tail rotor, are shown in Figure 19 through 22, respectively. The hover spectrum was taken with the tail rotor near its mid position.

In the hover spectrum, the sound pressure levels of the 2nd and 3rd harmonics are seen to be well above (more than 10 dB) those of the reference configuration (Figure 6), while the 5th through 10th harmonics are about 5 dB above those of the reference configuration. At $\mu = 0.09$, large differences in sound pressure levels between this and the reference configuration are noted in the 1st through the 6th harmonic, and the differences tend to decrease with harmonic numbers above the 6th harmonic. Above $\mu = 0.09$ the noted differences tend to diminish with increasing advance ratio.

The noted characteristics of the noise produced by the pusher configuration appears to stem from the peculiarities of the configuration rather than from main rotor wake/tail rotor interaction characteristics. A significant difference in the spectra between the tractor and the pusher can be seen in hover, for example, where no interactions occur. These peculiarities, in turn, stem from the difference in the blockage effect, whether the blockage occurs on the inflow or the downwash side of the tail rotor disk. Geometrically, it would be expected that some flow distortion would be effected in the main rotor wake by the fin blockage mode. It is not believed that this distortion effects any significant changes in the interaction characteristics. More plausibly, it appears that the interaction peaks are less significant on a relative basis in comparison to say, the reference configuration.

F. Configuration 6 - Effect of Change in Direction of Rotation

The direction of rotation of the tail rotor of the reference configuration was such that the upper side was the advancing side of the disk. For this configuration, the upper side was the retreating side of the disk. Noise spectra in hover and at advance ratios of 0.09, 0.20 and 0.28 for the tail rotor in its full-down position are shown in Figures 23, 24, 25 and 26, respectively. The hover spectrum was taken with the tail rotor near its mid position.

The harmonics of the tail rotor noise in the hover spectrum are not as pronounced for this configuration as they were for the reference configuration (Figure 6) in that only the 4th and 5th harmonics are dominant. The spectra at $\mu = 0.09$ and $\mu = 0.20$ were characterized by rather uniform sound pressure levels in the range from 70 to 75 dB for the first five harmonics of the tail rotor blade passage frequency, with a sharp drop-off of at least 10 dB above the fifth harmonic. This distribution of harmonic peaks is significantly different from that of the reference configuration at the same advance ratios. For the reference configuration, there was generally only one dominate peak below the fifth harmonic with significant harmonic peaks through the 9th. This dominance of the lower harmonics was less pronounced at $\mu = 0.28$, as the sound pressure levels of the 6th through the 9th harmonics increased more sharply than the 1st through 5th, while the sound pressure level of the 4th harmonic dropped off. The dominance of the lower harmonics in the noise spectra at $\mu = 0.09$ and 0.20 was also exhibited by Configuration 4, in which the fin blockage area was reduced from 25% to 13%. The noise characteristics of the tail rotor, regardless of main rotor wake interaction characteristics, appear to be sensitive to relatively small changes in local flow conditions and modified by advance ratio.

Figures 27 and 28 show the spectra for the tail rotor near its full-up position at advance ratios of 0.09 and 0.20, respectively. In this tail rotor position, main rotor wake/tail rotor interactions would occur on the lower, or advancing side of the tail rotor disk. Comparison of the spectra at $\mu = 0.09$ for the two extreme vertical positions of the tail rotor (Figures 24 and 27), show only slight differences in the sound pressure levels in the first 5 harmonics. With the tail rotor up, however, the 6th and 7th are noticeably increased above those shown with the tail rotor down. In addition, with the tail rotor in its up position, peaks can be seen in the spectra through the 6th harmonic of the tail rotor blade passage frequency, which are associated with the sum of the tail rotor and main rotor frequencies. This phenomenon is noteworthy, since for the reference configuration at the same conditions (Figure 8), the same type of peaks were manifest at the difference of the tail and main rotor frequencies. The characteristics of the noise produced by the tail rotor can thus be noted to be quite sensitive with respect to the direction of tail rotor rotation in relation to the points of interaction of the main rotor wake with the tail rotor.

At microphone positions forward of Microphone 4, the peaks in the spectra were a little more pronounced through about the 10th harmonic. This characteristic is shown in Figure 29 for Microphone 2 for the full-down position of the tail rotor at an advance ratio of 0.20, and similar characteristics were noted at advance ratios of 0.09 and 0.28. Figure 30 shows the spectrum for

the same conditions as in Figure 29, except that the tail rotor was near its full-up position. Analysis of these data indicate the expected type of behavior of main rotor wake/tail rotor interaction noise; that is, a directivity along the flight path of the helicopter and a pronounced effect of the sound pressure levels where the interactions occur on the advancing side of the tail rotor disk.

On the basis of the data analyzed for this configuration in comparison to that for the reference configuration, it is concluded that the direction of tail-rotor rotation is one of the primary parameters in the main rotor wake/tail rotor interaction phenomenon, and which showed a sensitivity with advance ratio.

G. Configuration 7 - Effect of Change in Tail Rotor Tip Speed

An increase of one-third in the nominal tip speed of the rotor was effected by installing a 0.254m diameter rotor in lieu of the reference 0.1905m diameter rotor, while maintaining the rotational speed constant. The collective pitch angles of the larger diameter rotor were reduced to obtain approximately the same thrust as that of the reference tail rotor. The reduction in collective pitch was also mandated as the tail boom had to be extended further aft to preclude physical interference of the tail rotor with the main rotor. The longitudinal separation between the disk planes of the main and tail rotors was maintained at about one-half of the main rotor chord. It should also be noted that because of the finite length of travel in the vertical positioning mechanism of the tail rotor, the main rotor wake/tail rotor interactions occurred nearer the center of the tail rotor disk for this configuration, as opposed to all other configurations. For consistency in discussion, however, the vertical position has been referred to as either up or down. Noise spectra in hover and at advance ratios of 0.09, 0.20 and 0.28 for the tail rotor in its down position are shown in Figures 31 through 34, respectively. The hover spectrum was taken in the tail rotor at approximately its mid position.

The spectrum in hover has several notable characteristics as for example, the secondary peaks in the sound pressure levels in the harmonics above the third. These are not associated with any effects of main rotor wake interaction as the peaks were also noted in the spectra taken when the main rotor speed was zero. These peaks were noted primarily in Microphones 3, 4 and 5. It is also seen that peaks occur at the rotational frequency of the tail rotor, and although these were noted in the spectra of the 0.1905m diameter rotor, they were not as pronounced for the smaller rotor as they were in this configuration. As noted previously, the peaks in the spectrum at the rotational frequency of the blade were associated with asymmetries in the blades, and this

condition probably effected the secondary peaks in the spectrum associated with the blade passage frequency. Comparison of this hover spectrum with that of the reference configuration (Figure 6) shows that the first four harmonic peaks in the spectrum are about 10 dB above those of the reference configuration while the harmonic peaks in the range of 5 through 10 are less pronounced. This increase is directly attributable to the higher tip speed of the rotor.

In forward flight, the effects of the higher tail rotor tip speeds were quite pronounced at all advance ratios. At $\mu = 0.09$, for example, (Figure 32) the differences in the sound pressure levels are quite pronounced throughout the spectrum ($\simeq$10 dB) which made the harmonics above the 6th much more pronounced than those of the reference configuration, (Figure 7). At $\mu = 0.20$ (Figure 33), pronounced differences in the sound pressure levels were also noted primarily above the 6th harmonic, while at $\mu = 0.28$, these differences were noted primarily above the 7th harmonic. Comparison of the spectra of the reference configuration with those of this configuration generally indicates that while there are measurable differences in the lower harmonics of the tail rotor blade passage frequency, relatively large differences in harmonics above the 6th are realized. Analysis of the noise spectra of other microphones showed similar results, although the differences were not as pronounced upstream (say at Microphone position 2) as they were at Microphone position 4 (as shown in Figures 32 through 34). For Configuration 7, the tail rotor thrust was approximately equal to that of Configuration 1. The area was increased by a factor of about 1.8, so that the disk loading was smaller. It might have been expected that this condition, coupled with the increase in tip speed, would have maintained the sound pressure levels of the two configurations about the same. The noise characteristics, however, appear to be more sensitive to tip speed than to disk loading, particularly for harmonics above the 6th.

The effects of main rotor wake/tail rotor interactions were difficult to sort out for this configuration. In part this was due to the fact that the interactions for this configuration occurred nearer to the center of the disk than those of all other configurations. In this condition, as with the tail rotor in either the mid or down position for the standard size tail rotor, the noise characteristics appeared to be affected more by the turbulent flow of the main rotor wake, rather than by interaction with the main rotor wake vortexes, per se.

On the basis of the data obtained with the larger diameter tail rotor it could not be definitively concluded whether higher rotor tip speeds could enhance the quantitative analysis of the noise phenomena produced by main rotor wake/tail rotor interactions. One of the reasons stems from the fact that direct comparisons of the data in terms of tail rotor positions could not

be made as with other parametric changes. One of the advantages noted with the higher tip speed rotor, however, was that the sound pressure levels could be analyzed over an extended range of the frequency, as the noise levels were more above the background noise levels at the higher frequencies. A disadvantage, however, stems from the constraint of wind tunnel velocities to about 30 m/sec, where with high tip speed rotors, data can only be obtained at low advance ratios.

H. Configurations 8-1 and 8-2 - Effect of Changes in Rotor Tip Speed Ratios

Changes in rotor rotational speed ratios were effected by changes only in the rotational speed of the tail rotor. Two variations were made from the 5.1:1 rotational speed ratio of the reference configuration. In the first variation (Configuration 8-1) the tail rotor speed was reduced 10 percent from that of the reference configuration, which provided a rotational speed ratio of 4.6:1, and in the second variation, the tail rotor speed was fixed at an integer multiple of the main rotor speed, that is, at 5.0:1.

A noise spectrum for Configuration 8-1 for one microphone position, at an advance ratio of 0.20 and for the full-down position of the tail rotor, is shown in Figure 35. The peaks in the spectrum are more closely spaced than in the reference configuration because of the drop in rotational speed, but the sound pressure levels of the same harmonic order are about the same for this configuration up to about the 8th harmonic. Similar results were noted at advance ratios of 0.09 and 0.28, and at the other microphone positions.

Noise spectra for Configuration 8-2, in which the tail rotor rotational speed was an integer multiple of the main rotor rotational speed are shown in Figures 36 and 37. Spectra are shown for an advance ratio of 0.20, for two microphone positions and for two positions of the tail rotor. As noted previously, this configuration was run to provide base data for correlation with a rotor noise predictive theory. In this configuration, true periodicity can be assumed in the interaction of the main rotor wake with the tail rotor. Since there was only about a 2% difference in the rotational speeds of the tail rotor between the two configurations, only slight differences in the sound pressure levels between this and the reference configuration would be expected. This expectation was largely borne out in the results, although a few sporadic differences appear in the sound pressure levels, which might be due to some randomness in the phenomena. A further discussion of the results obtained with this configuration is presented in a succeeding section of this report.

I. Configuration 9 - Effect of Change in Main Rotor Thrust

Configurations 1 through 8 were tested with the main rotor thrust coefficient approximately equal to 0.005. In Configuration 9, the thrust coefficient was increased to about 0.007. The tail rotor thrust was increased commensurately (see Table III). The spectrum for the hover condition of this configuration is shown in Figure 38 and a spectrum at an advance ratio of 0.20 for the full-down position of the tail rotor is shown in Figure 39. In comparison of the hover spectrum with that of the reference configuration (Figure 6) at the lower frequencies, it is seen that the main rotor rotational noise peaks have increased with the increased thrust coefficient, which tends to obscure the lower harmonics of the tail rotor noise peaks. Most of the sound pressure levels of the first 10 harmonics of the tail rotor rotational noise are within 2 dB between the two configurations. The 5th and 6th harmonics of Configuration 9, however, are down 3 and 5 dB over that of Configuration 1. This result is inexplicable, as it would be expected that some increase would be shown in all harmonics, although the increase would probably have been within the experimental error.

The spectrum at an advance ratio of 0.20, Figure 39, shows somewhat more consistent results, as the sound pressure levels of most harmonics of the tail rotor noise have shown an increase from those measured for Configuration 1. The sound pressure level of the 1st harmonic for Configuration 9 was slight below that of Configuration 1, while the 5th was about the same for both configurations. The spectra at $\mu = 0.09$ and $\mu = 0.28$ were also consistent with those of Configuration 1, generally showing slight increases in the sound pressure levels. At $\mu = 0.09$ with the tail rotor in the up position, peaks at the difference of the tail and main rotor frequencies were also evident in the spectra, as were noted in those of Configuration 1, and discussed previously.

The experimental data obtained with the various test configurations has shown that many parameters affect the noise characteristics of the tail rotor. Although the effects of main rotor wake/tail rotor interactions on the noise characteristics of the tail rotor were of primary interest in the program, it has been established, not unexpectedly, that other parameters have a pronounced effect on these noise characteristics as well. In spite of the volume of data that were collected, it would be presumptuous to conclude that definitive trends in relation to tail rotor noise characteristics were established. The experimental results however, have defined some of the more significant parameters that affect the noise characteristics of the tail rotor. As the model has been demonstrated to be a versatile tool for the experimental investigation of tail rotor noise, it is believed that further model investigations can develop the type of data that could establish more definitive insights into the mechanisms associated with tail rotor noise, and hopefully, lead to the alleviation of the tail rotor noise problem.

THEORETICAL ANALYSES OF INTERACTION NOISE

The noise produced by the interaction of the main rotor wake with the tail rotor is one of the major sources of noise of the helicopter. Accurate prediction of the noise produced by this interaction depends on an accurate description of the aerodynamic forces that are imposed on the tail rotor during the interaction. The description of these aerodynamic forces requires suitable analysis techniques for the prediction of the nonuniform aerodynamic environment in which the tail rotors operate. The essence of such techniques lies in existing analyses which can represent the nonuniform wake induced velocity effects on helicopters with multiple rotors. As far as is known, however, most of these techniques are not directly applicable to the main rotor wake/tail rotor interaction problem because

1. the rotational speed of the tail rotor is not equal to, or an integer multiple of the main rotor speed.

2. the analysis does not account for the aerodynamic interference caused by the fin.

3. the incremental azimuthal step size needed to adequately represent some interactions is much smaller than generally considered in existing analyses for helicopters with multiple rotors.

In spite of these limitations, existing techniques can be used to provide a reasonable description of the noise produced by the interaction of the main rotor wake with the tail rotor. The manner in which such techniques were utilized to accomplish this prediction is described below.

The basic tools that were used to predict some of the main rotor/tail rotor interaction phenomena were a freely-deforming wake analysis (Reference 3) and a rotor noise predictive method (Reference 4). The rotor noise prediction technique calculates the acoustic pressures emitted by the motion of a rotor blade in a time frame. The technique calculates the rotational noise produced by the blades, which is associated with the lift and drag forces developed by the blade, as well as the vortex noise which is associated with discrete vortex shedding along the blade. The analysis also accounts for the effects of ground reflection, the variability of the oscillatory forces as related to vortex shedding and for the simulation of certain vortex interaction phenomena. Such a simulation, for example, was used to predict the noise produced by a full-scale main rotor in hover assuming a periodic interaction with its own trailed vortex (Reference 5). The freely-deforming wake analysis computes the spatial positions of rotor wakes, as well as the induced velocities at arbitrary points in space that are effected by the wakes. The analysis accounts for

the mutual and self-induced effects of the wake in calculating the spatial positions.

The freely-deforming wake analysis was used to determine the main rotor wake position and the strengths of the vortexes that were located in the tail rotor disk. The input parameters to the wake analysis were those of Configuration 8-2 at an advance ratio of 0.20 (see Table III). Once the position of the wake was defined, the interactions could be realistically assumed to occur anywhere within the envelope described by the tail rotor positioning mechanism. The paths and spacings of the vortexes which would interact with the tail rotor, that is, those trailed off near ψ = 0 and 180°, in terms of three vertical tail rotor positions, are shown in Figure 40. The vertical positions of the tail rotor are those corresponding to its down, mid, and up positions. A noteworthy characteristic of the wake was the trajectory of the vortex trailed off near ψ = 180°, in that its vertical spacing with respect to the vortex trailed off near ψ = 0 was rather small. As a matter of interest, its path was traced from its shedding point at ψ = 180°. The vortex was swept downward initially, but was brought up toward the disk plane of the main rotor on the aft portion of the disk, which also brought it into the proximity of the vortex that was trailed off near ψ = 0. The maximum tangential velocities and the sense of the circulation of the vortexes also differed. The maximum tangential velocity of the vortex trailed off near ψ = 0 was about 40 percent of the rotor tip speed, while that of the vortex trailed off near ψ = 180° was about 30 percent of the rotor tip speed.

Although the wake analysis described the trajectories and relative locations of the vortexes, the phasing of the tail rotor blades with these vortexes could be quite arbitrary. Many types of interactions can be considered in the analyses. For example, it can be assumed that only either one of the vortexes is convected through the disk plane of the tail rotor, or that both are convected through. In one case, it can be assumed that the first interaction occurs when the center of the vortex is located at the tip of the tail rotor blade as shown for the ψ = 0 vortex in Figure 40. In another case, it can be assumed that the first interaction occurs when the center of the vortex that was trailed off near ψ = 180° is aligned with the tip of the rotor blade. The spacing between the vortexes, however, should be assumed to be that predicted by the wake analysis, as also shown in Figure 40.

With a 5:1 ratio of tail rotor-to-main rotor rotational speeds and at an advance ratio of 0.20, the vortexes from the main rotor would be swept through the disk plane of the tail rotor in about 2 1/2 revolutions of the tail rotor. It was thus assumed that the phenomenon was periodic every 2 1/2 revolutions of the tail rotor. Effects due to phenomena such as vortex shedding, ground reflection, etc. were not included in the analyses. The rotational

noise of the main rotor was also not included in the analyses that are presented in the succeeding discussion. Preliminary analyses showed that the main rotor noise would effect only minor differences in the results while the essence of the analyses was directed toward prediction of the changes in the tail rotor noise characteristics.

The characteristics of the sound pressure as a function of time assuming uniform inflow for the tail rotor, and for the interaction of the two main rotor vortexes with the tail rotor are shown in Figure 41. In this case, the interaction was assumed to be periodic, as noted in the pressure time history. The maximum instantaneous value of the pressure pulse due to the interaction of the main rotor vortex trailed off near $\psi = 0$ was increased by a factor on the order of 10 above that of the rotational noise pulse. There were, however, four interactions of each of the two vortexes of the main rotor in every revolution of the tail rotor. The effects of the pressure pulses due to the initial interactions were much greater than the succeeding ones as the initial interactions occurred in the forward section of the disk, and on the outboard section of the blade.

The spectrum for the pressure time history shown in Figure 41 is shown in Figure 42. As might be expected because of the simplifying assumptions made in the analysis, only the sound pressure level at the blade passage frequency is reasonably representative of that measured experimentally. The spectrum also exhibits noise peaks at harmonics of the main rotor blade passage frequency which are due to the assumption of periodicity. Interaction noise peaks are also noted as the main rotor vortex was swept through the disk plane of the tail rotor. It was also not surprising that the experimental data for the "periodic" case where the tail rotor rotational speed was an integer multiple of the main rotor rotational speed did not exhibit peaks in the spectra at evenly spaced frequency intervals. This stems from the fact that true periodicity is difficult to achieve in practice, except, perhaps, for short periods of time. As the spectra were averaged over relatively long periods, the theoretical type of peaks in the noise spectra would not be evident.

This simplified representation of the rotor model was used, however, to determine whether the effects of some of the parametric model changes could at least be correctly predicted on a qualitative basis. These results are summarized in Table IV which follows.

TABLE IV QUALITATIVE COMPARISON OF EXPERIMENTAL RESULTS WITH SIMPLIFIED THEORY

PARAMETER	GENERAL TREND OF NOISE LEVELS	
	EXPERIMENT	THEORY
Increase in main rotor tip vortex strength	Little Change	Increase
Main rotor wake interactions on advancing (upper) side of tail rotor disk	Increase	Increase
Main rotor wake interactions on advancing (lower) side of tail rotor disk	Increase	Increase

As can be noted from the table, the theory showed a slight increase in the noise levels with an increase in the main rotor tip vortex strength which intersected with the tail rotor. The experimental data showed only a slight change in the spectra. The theoretical results also showed a sensitivity to the points of main rotor wake interaction on the tail rotor disk, showing an increase when the interactions occurred in the advancing or upper side of the tail rotor disk for the reference configuration, and a corresponding decrease when the interaction occurred as the lower or retreating side. When the direction of rotation was reversed, the experimental data showed a marked increase in the noise levels, and this characteristic was also correctly predicted theoretically. In addition, the directivity of the noise emitted by the tail rotor also showed the same general trend as had been observed experimentally.

Notwithstanding these results, however, it was quite evident that the theoretical noise predictions were quantitatively inadequate for comparison with experiment. Efforts were then directed to determine the effects of some parameters which are known to be pertinent in the interaction noise phenomena.

These efforts were not only directed to seek improvement in the quantitative prediction of interaction noise, but also to determine the extent of sophistication that might be required

for adequate prediction of these noise phenomena. The two basic parameters that were investigated were the effects of nonperiodicity in the main rotor wake/tail rotor interaction and the effects of a nonuniform tail-rotor wake.

In conventional helicopters, the rotational speed of the tail rotor is not an integer multiple of the rotational speed of the main rotor. This condition can effect a significant change in the pressure time history and in the resultant spectrum. Figure 43, for example, shows the pressure time history of an interaction comparable to that shown in Figure 41, but assuming a nonperiodic characteristic of the interaction ($\Omega_{TR}/\Omega_{MR} \simeq 5.1$). The position of the first interaction of the main rotor vortex on the tail rotor disk, however, was assumed to be the same as that shown in Figure 41. In each succeeding interaction of the same vortex, the characteristic periodicity is not evident as there is a phase shift in the peak pressure pulse with respect to the rotational noise peaks due to the interaction. The change in the spectrum that is effected by the nonperiodicity is shown in Figure 44. The spectrum is obviously more akin to those which were obtained experimentally in that the harmonics of the main rotor rotational speed are not as pronounced at each harmonic as they were in the case where periodicity was assumed (Figure 42). Also there is a slight improvement in the prediction of the 2nd harmonic of the tail rotor rotational noise. Absolute correlation between these results and the experimental data would be inappropriate, however, because of the simplifications made in the analysis.

One of the other pertinent considerations in predicting rotor noise phenomena is the effects due to the nonuniform tail rotor wake per se. In the analysis discussed above, only uniform inflow was assumed for the tail rotor. The effects of a nonuniform induced velocity distribution of the tail rotor were also investigated. These effects were derived from scaled values of induced velocity distributions of larger untwisted rotors.

The noise spectrum showing the effects of the nonuniform induced velocity distribution and the interaction of the nonperiodic main rotor wake is shown in Figure 45. The spectrum is shown in Figure 45. The spectrum is characterized by the distinctness of the tail rotor rotational noise peaks, as had been manifested in the experimental results. The magnitudes of the sound pressure levels are also more consistent with those measured experimentally. It would also be inappropriate to correlate the "theoretical" noise data with that obtained experimentally, as the effects of the various phenomena that were believed to be pertinent to the tail rotor noise characteristics were included rather coarsely in the analysis and the analysis did not include other phenomena which are also pertinent to the problem.

The analysis and its results as discussed above were intended primarily to determine the extent to which existing techniques of noise prediction could be applied to predict main rotor wake/tail rotor interaction phenomena. The prediction of the absolute values of the noise characteristics of main rotor wake/tail rotor interaction noise phenomena, however, is obviously highly complicated and requires the removal of the simplifying assumptions that were made in the analysis, as well as the inclusion of all other effects that are pertinent in the problem. In particular, it is believed that the superposition of the induced velocity of the main rotor wake on the tail rotor inflow would significantly affect the peak sound pressure levels of the tail rotor noise at harmonics above that of the blade passage frequency. In order to be able to predict the characteristics of the noise produced by the interaction of the main rotor with the tail rotor more quantifiably, it is believed that the following phenomena will need to be included in the analysis:

1. Main rotor noise
2. Effects of fin blockage
3. Definition of spatial positions of main rotor wake
4. Representation of nonperiodicity and arbitrary phasing in the interaction phenomenon
5. The induced velocity effected by the wake of the main rotor on the tail rotor inflow.
6. Nonuniform wake effects of the tail rotor
7. Determination of the effect of the incremental azimuthal step size in predicting the noise due to interaction phenomena.

CONCLUSIONS AND RECOMMENDATIONS

A research program was conducted in which a model was designed, fabricated and tested to identify some of the pertinent parameters that are relevant to main rotor wake/tail rotor interaction phenomena. The model, which was approximately a 1/16th scaled version of the UH-1 series helicopter, has been demonstrated to be a versatile tool for the collection of these as well as other noise data. The experimental data show that the interaction noise phenomena are intertwined with some of the geometric characteristics of tail rotor assemblies, as well as with some operating and flight parameters.

In general, the noise produced by the tail rotor was alleviated by increasing the spacing between the disk plane of the tail rotor and the fin. For the same spacing, the noise produced by the tail rotor was adversely affected when the tail rotor was operated in a pusher rather than in a tractor mode. The noise produced by the tail rotor was also adversely affected when the tail rotor direction of rotation was such that the rotational vector was to the right, rather than to the left. With the rotational vector to the right, the interaction peaks in the noise spectra were also affected, and would alter the subjective characteristics of the noise. An increase in tail rotor tip speed increased the noise levels produced by the tail rotor, per se, but appeared to have little effect on the interaction noise characteristics. Other parameters such as the longitudinal spacing between the disk planes of the main and tail rotors, changes in fin blockage area, tail rotor-to-main rotor rotational speed ratios and in the thrust coefficient of the main rotor showed less effect on the tail rotor noise characteristics than the parameters noted above. All parametric changes, however, showed a sensitivity of the tail rotor noise characteristics with advance ratio.

Analysis of the interaction noise characteristics using a simplified representation of the aerodynamic phenomena that occur during the interaction showed that existing techniques could be used to predict the pertinent noise characteristics with further refinement. The analyses were increasingly representative of the experimentally measured noise characteristics as the sophistication of the aerodynamic representation increased. Quantitative correlation of the experimental and theoretical noise characteristics was inappropriate as only the effects of a limited number of aerodynamic phenomena in the problem were investigated.

The research program has made it possible to widen the breadth and scope of investigations of main rotor wake/tail rotor interaction noise phenomena, as the model has been fabricated to be compatible with the anechoic test facility at NASA/Langley. In conjunction with testing which could further develop the characteristics of the interaction noise phenomena, it is recommended that theoretical development of these noise characteristics also be advanced. This type of bi-fold research effort would be most expeditious in advancing the understanding of the problem, which would lead to the alleviation of this noise source in modern helicopter development.

REFERENCES

1. Operations and Maintenance Manual for Helicopter Model for Parametric Model Study of the Noise Generated by the Aerodynamic Interaction of Helicopter Main and Tail Rotors. Aerosystems Research Division of Systems Research Laboratories, Inc. Note 16-76-1, December 1975.

2. Hayden, Richard E. and Kadman, Y.: Design and Performance of a High Speed Free Jet Acoustic Wind Tunnel. AIAA Paper 75-531, Presented at the 2nd Aeroacoustics Conference, Hampton, Virginia 24-26 March 1975.

3. Sadler, S. Gene: Development and Application of a Method for Predicting Rotor Free Wake Positions and Resulting Rotor Blade Air Loads. NASA Langley Report CR 1911, December 1971.

4. Johnson, H. Kevin: Development of an Improved Design Tool for Predicting and Simulating Helicopter Rotor Noise. USAAMRDL TR 74-37, June 1974.

5. Pegg, Robert J., Hosier, Robert N., Balcerak, John C. and Johnson, H. Kevin: Design and Preliminary Tests of a Blade Tip Air Mass Injection System for Vortex Modification and Possible Noise Reduction in a Full-Scale Helicopter Rotor. NASA TM X-3314, December 1975.

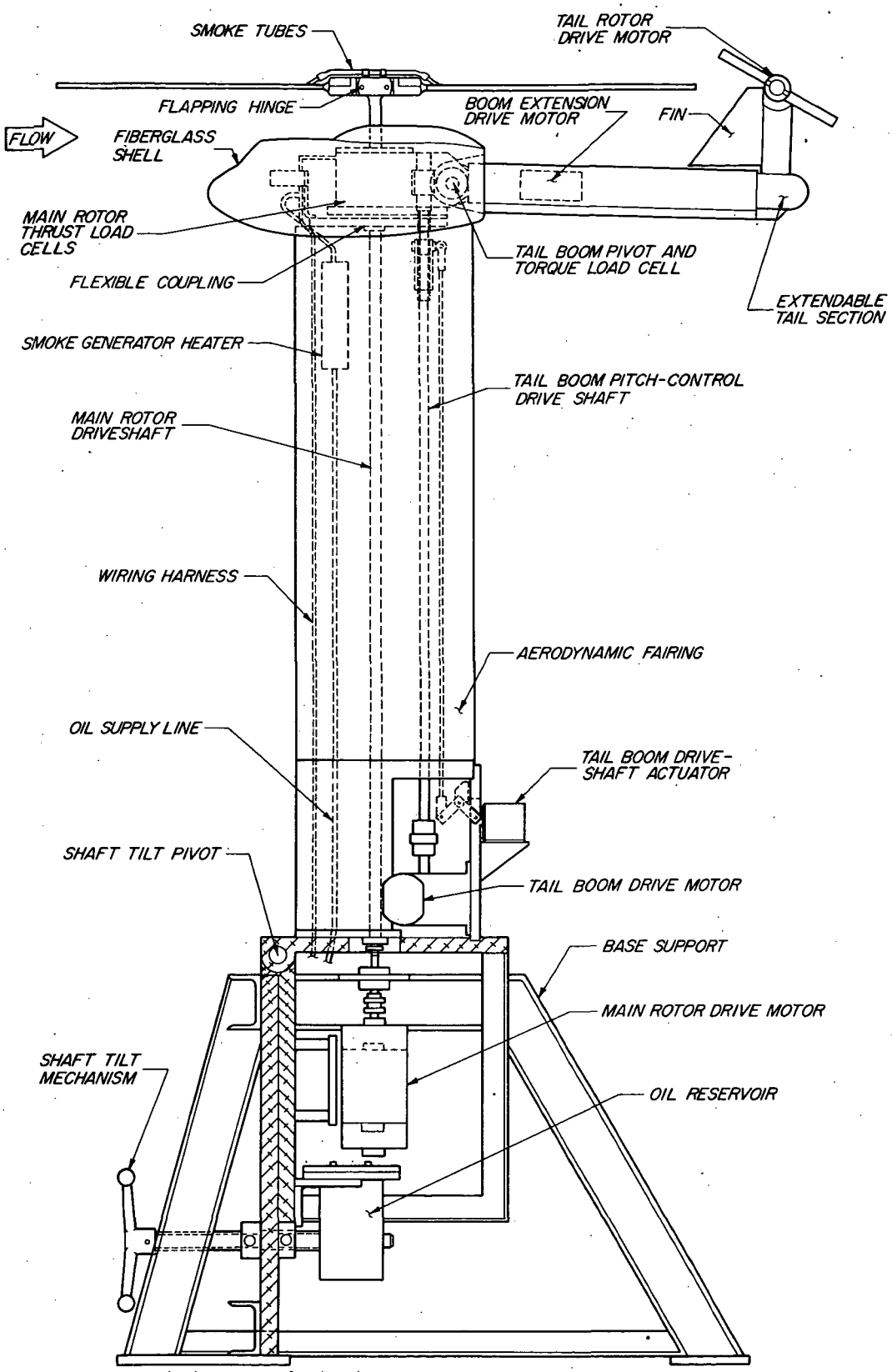

Figure 1. Schematic Diagram of Model and Support System

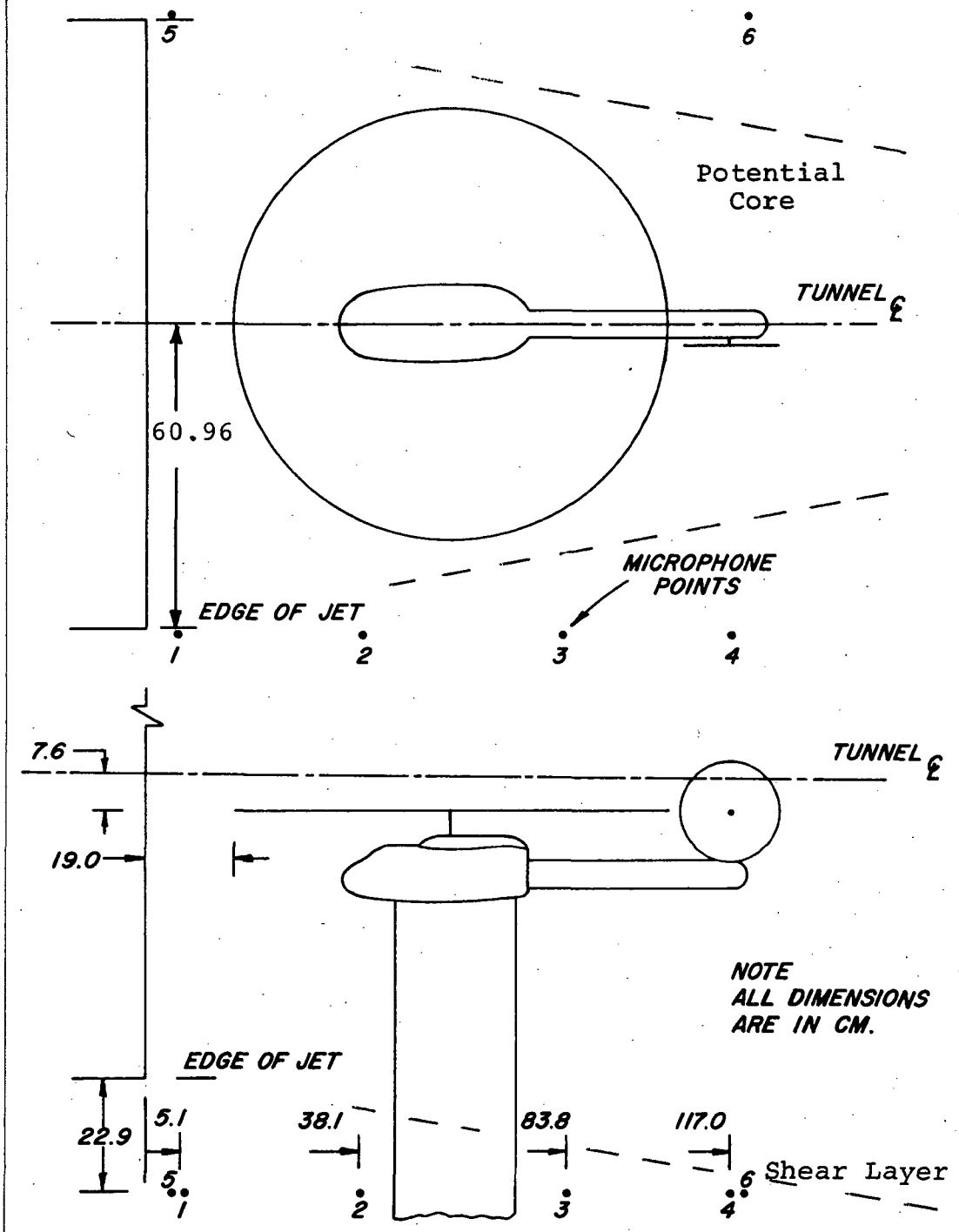

Figure 2. Schematic Diagram of Model Installation and Microphone Locations

Figure 3. Model Installation in Wind Tunnel

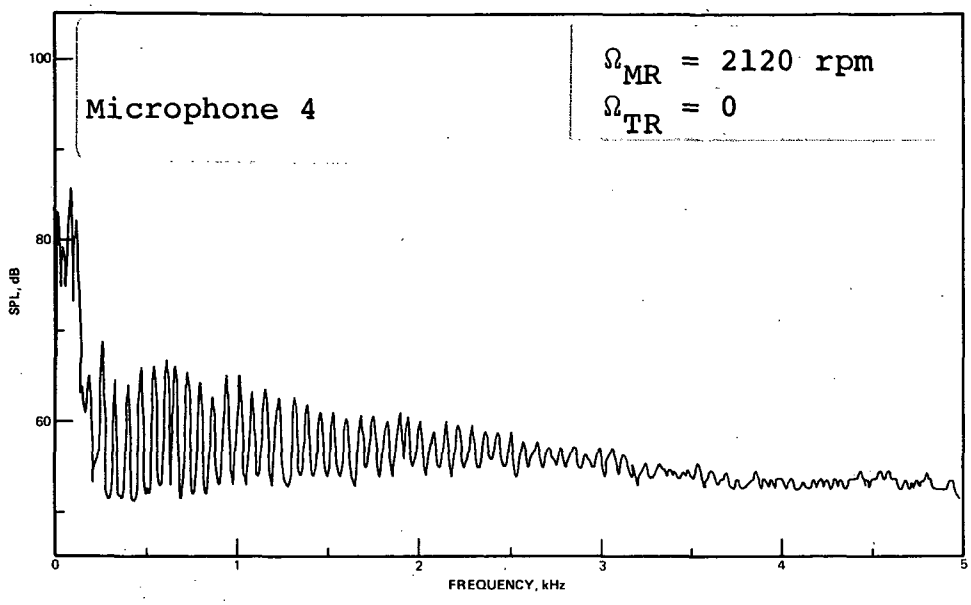

Figure 4. Measured Noise Spectrum of Main Rotor; V = 0

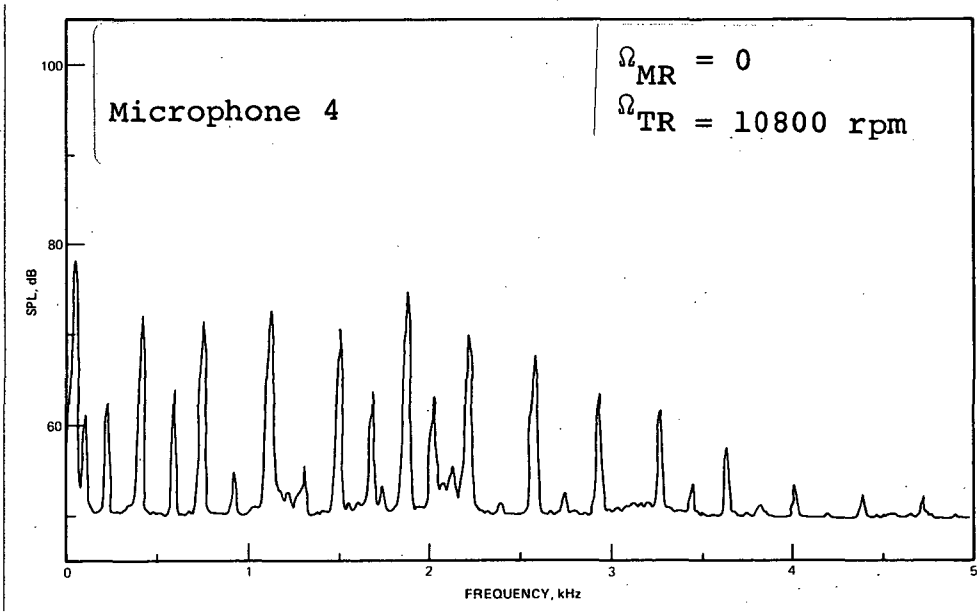

Figure 5. Measured Noise Spectrum of Tail Rotor; V = 0

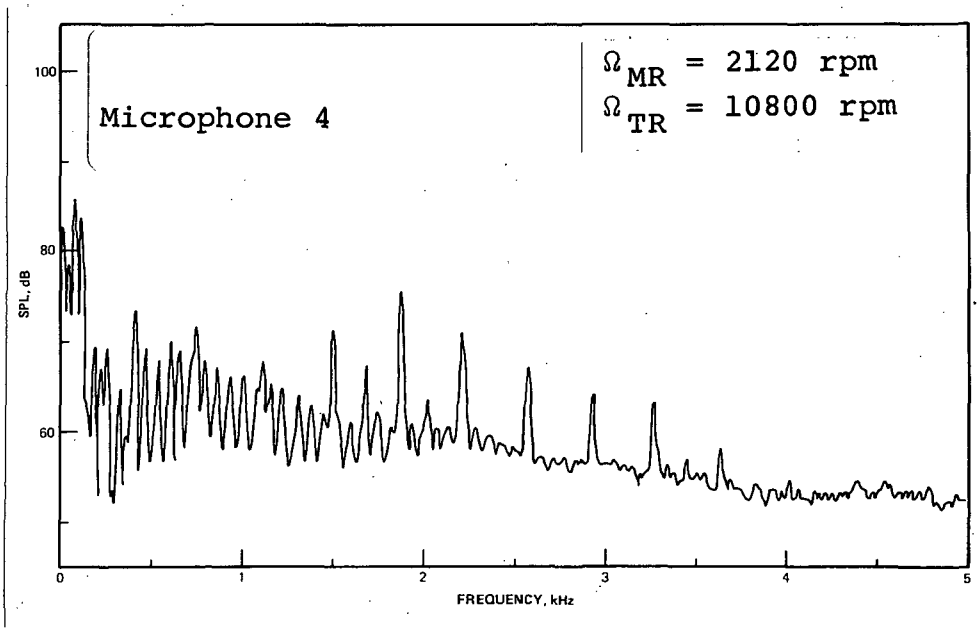

Figure 6. Measured Noise Spectrum of Configuration 1 in Hover

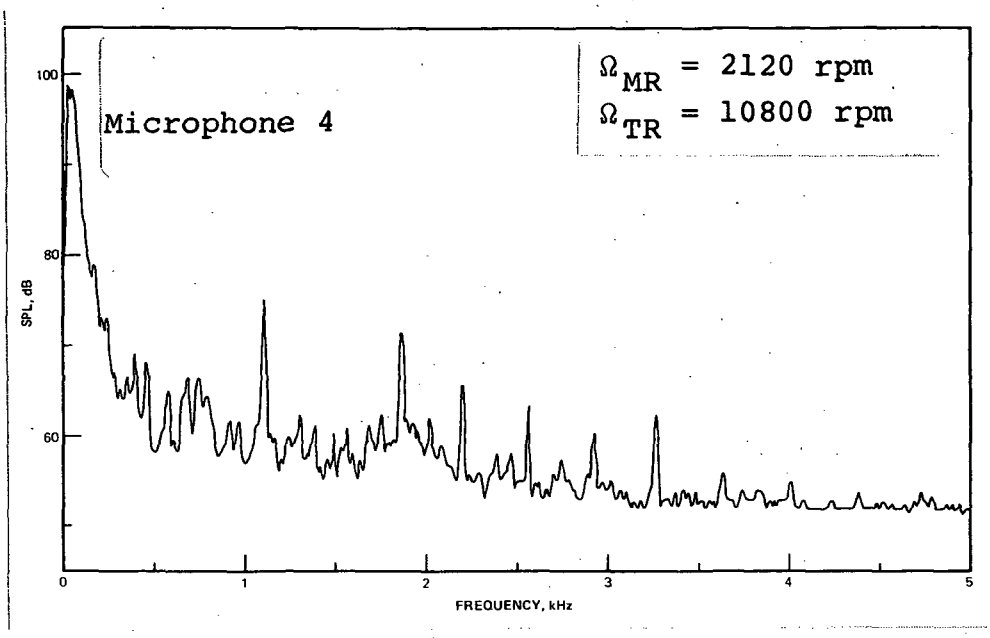

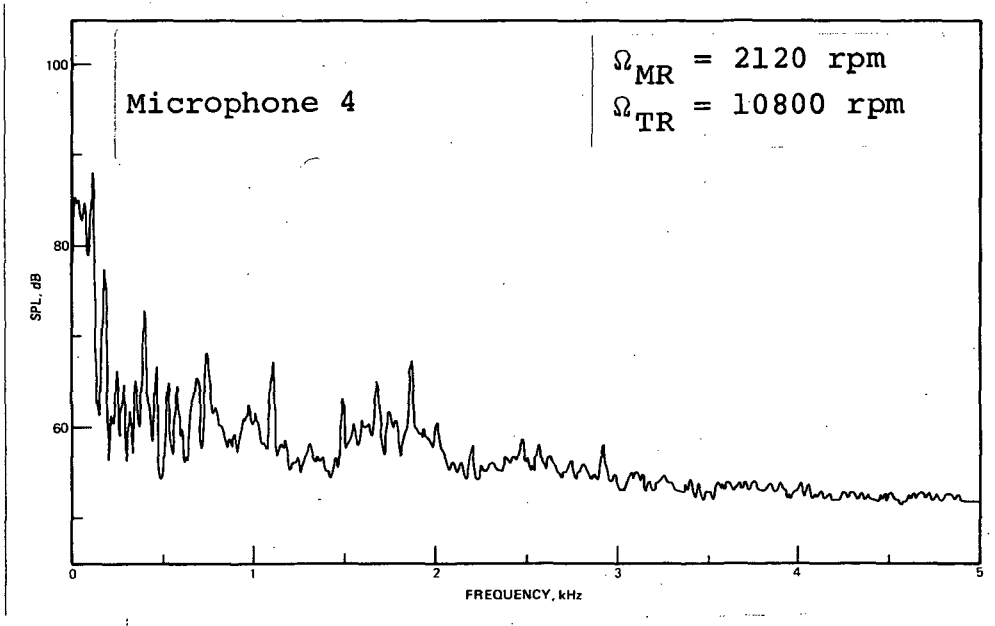

Figure 7. Measured Noise Spectrum of Configuration 1, μ = 0.09, Tail Rotor in Down Position

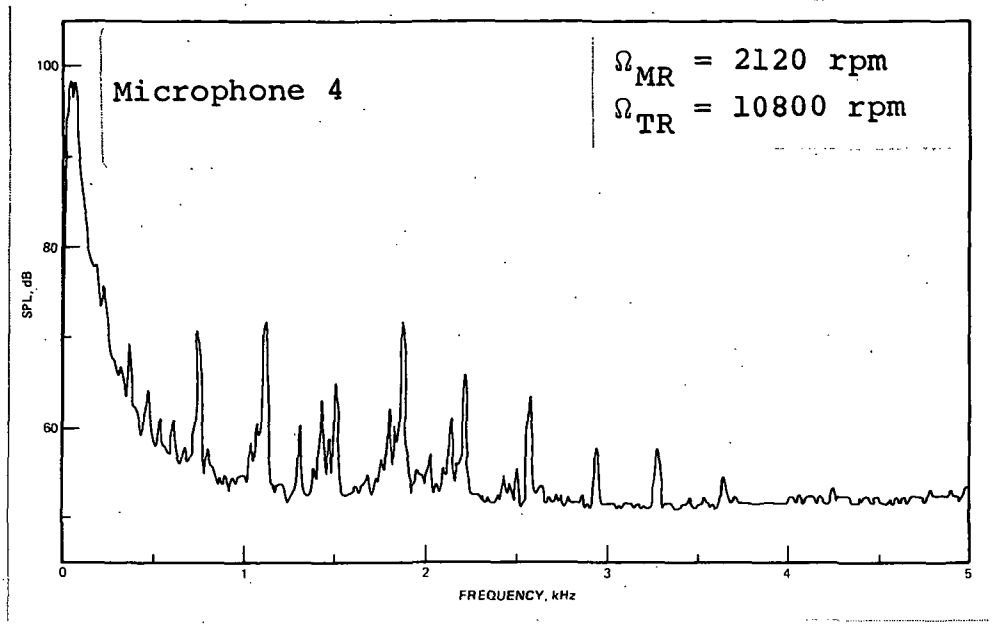

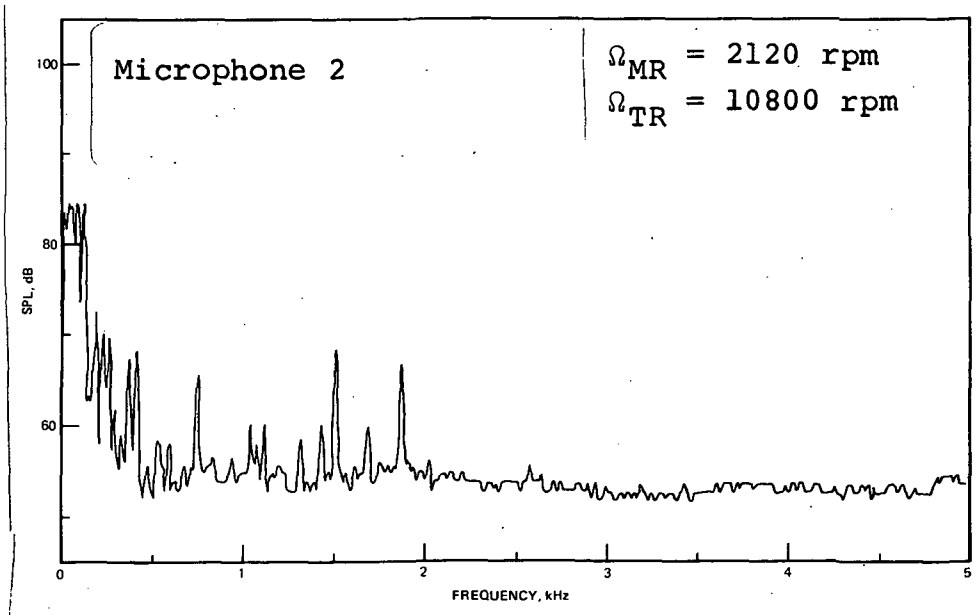

Figure 8. Measured Noise Spectrum of Configuration 1, μ = 0.09; Tail Rotor in Up Position

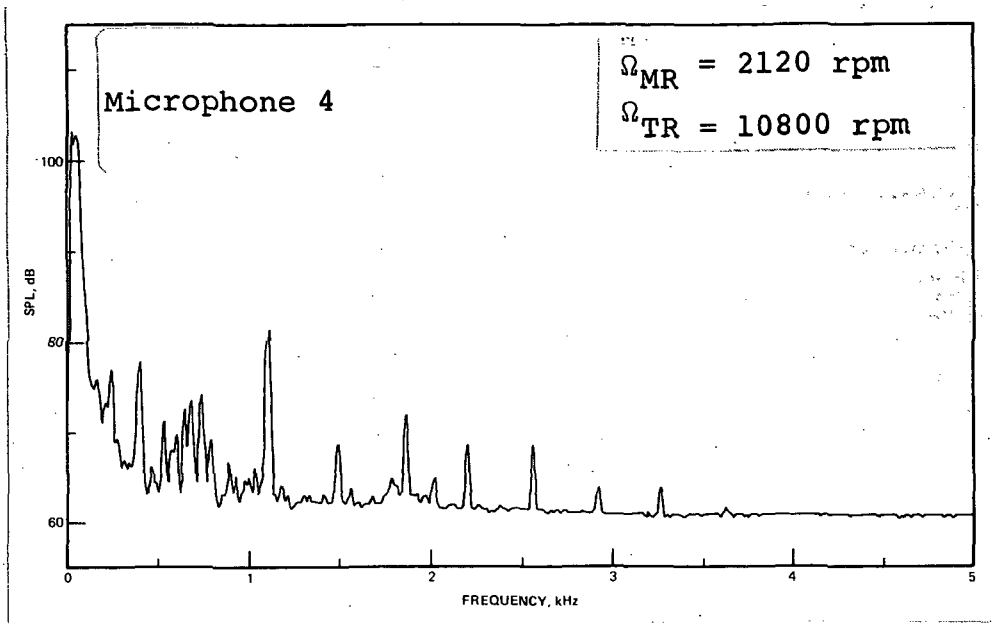

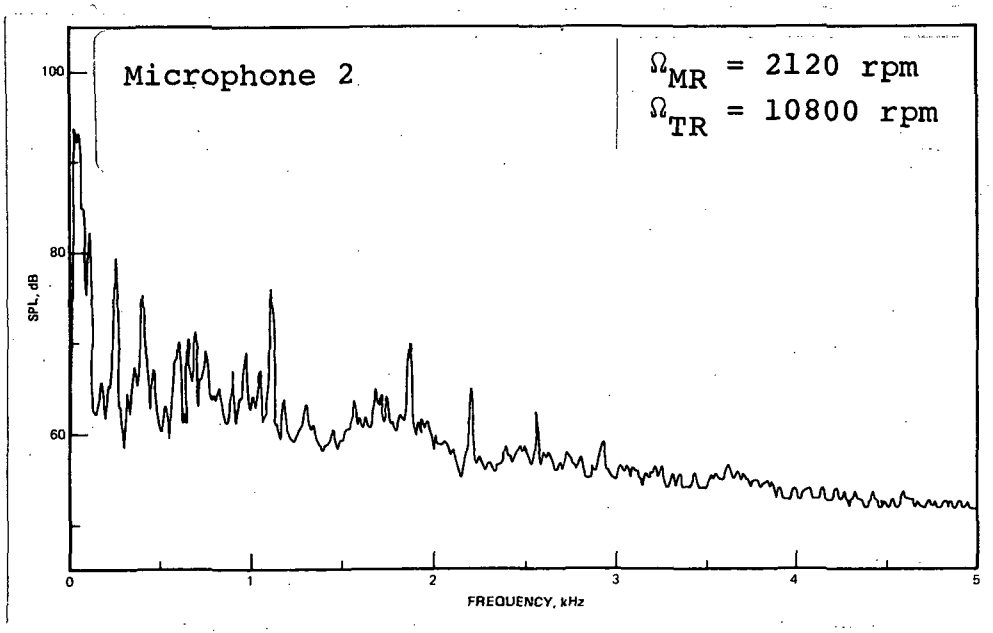

Figure 9. Measured Noise Spectrum of Configuration 1, μ = 0.20; Tail Rotor in Down Position

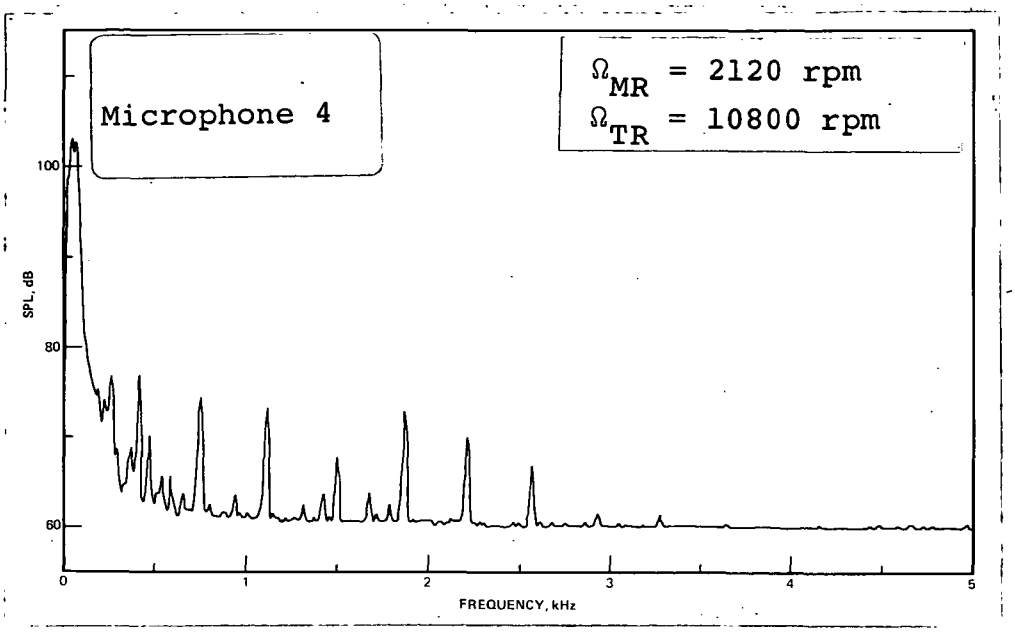

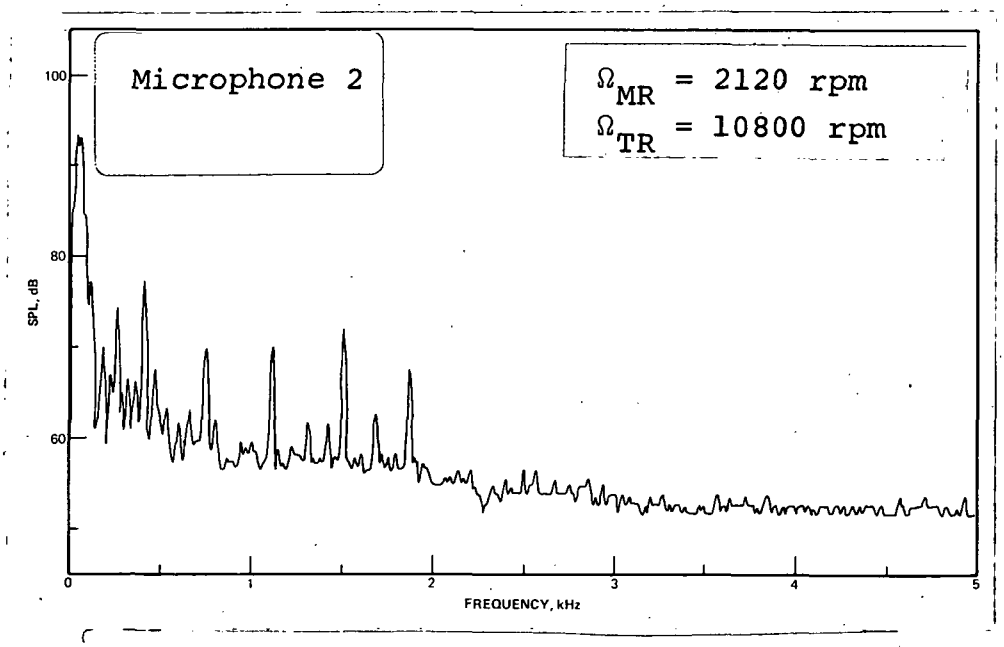

Figure 10. Measured Noise Spectrum of Configuration 1, μ = 0.20; Tail Rotor in Up Position

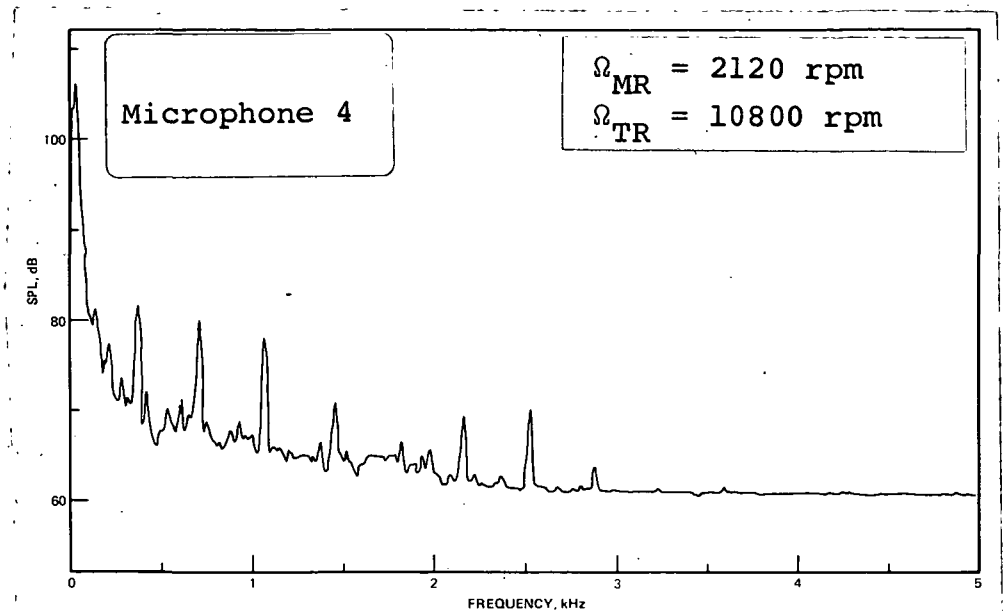

55-7

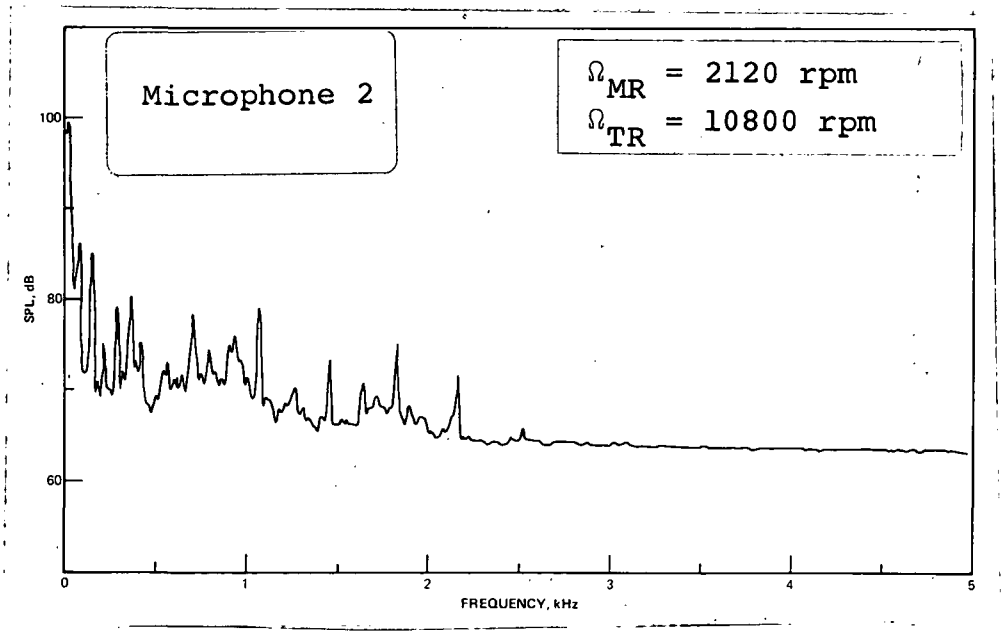

Figure 11. Measured Noise Spectrum of Configuration 1, μ = 0.28; Tail Rotor in Down Position

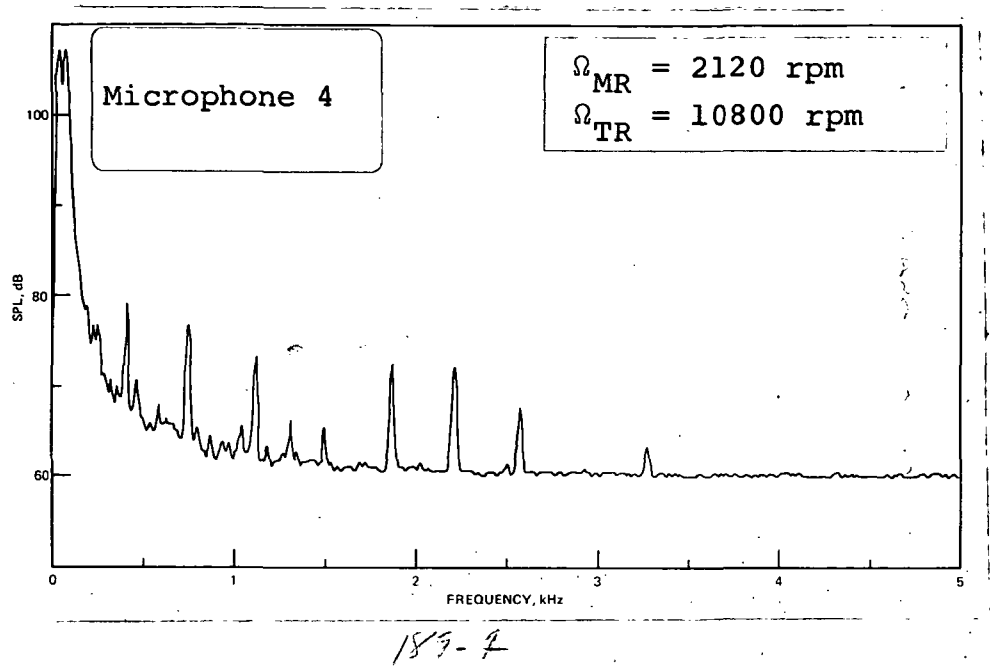

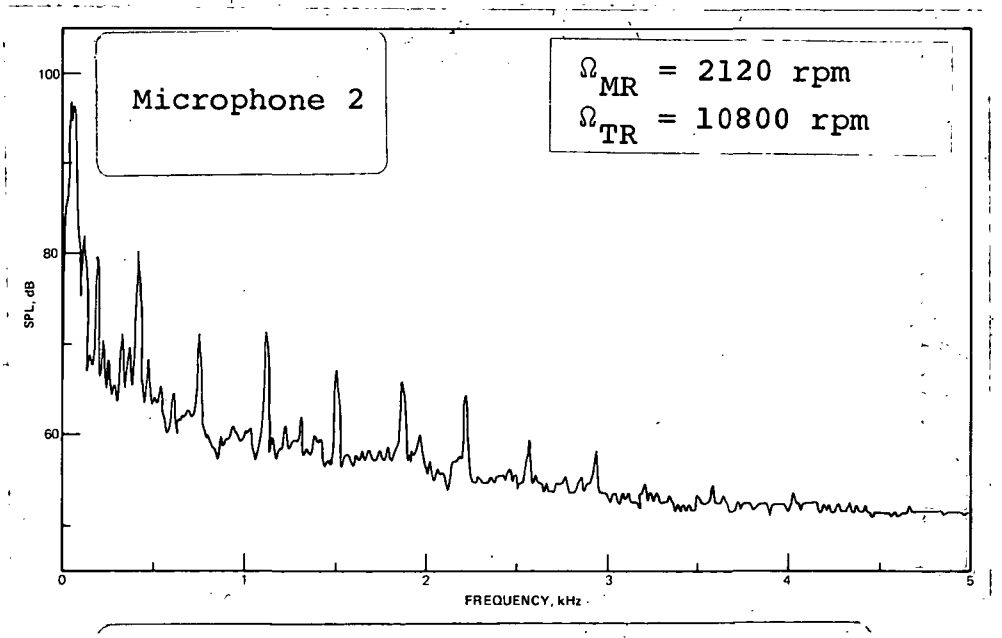

Figure 12. Measured Noise Spectrum of Configuration 1, μ = 0.28; Tail Rotor in Up Position

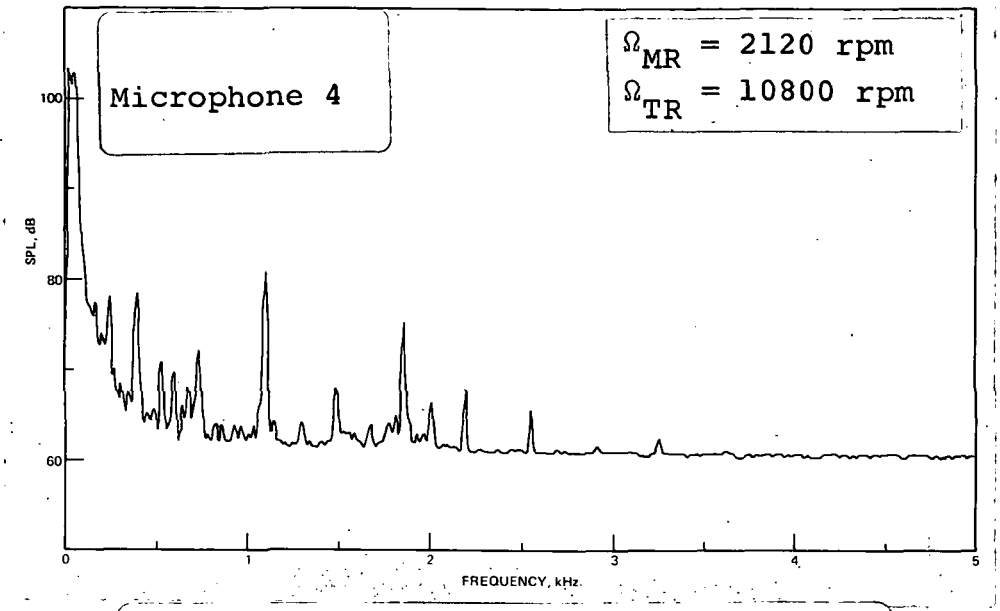

Figure 13. Measured Noise Spectrum of Configuration 2, μ = 0.20; Tail Rotor in Down Position

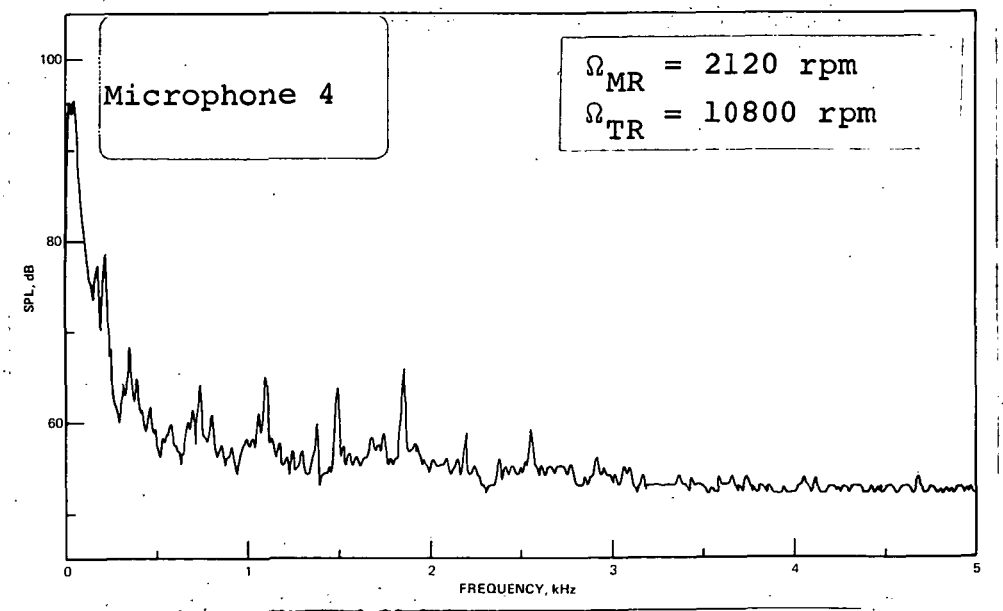

Figure 14. Measured Noise Spectrum of Configuration 3, μ = 0.09; Tail Rotor in Down Position

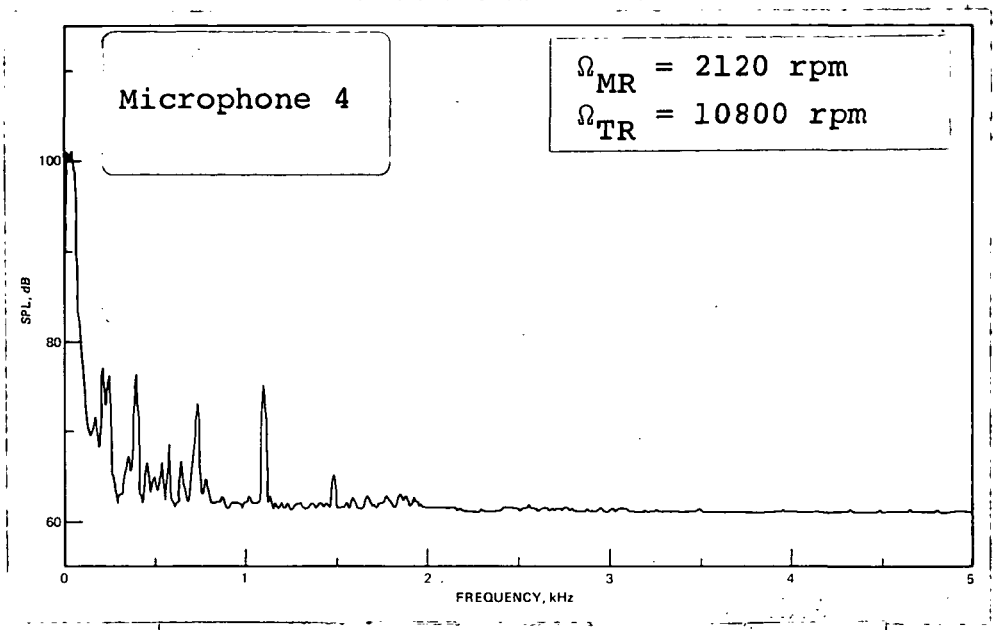

Figure 15. Measured Noise Spectrum of Configuration 3, μ = 0.20; Tail Rotor in Down Position

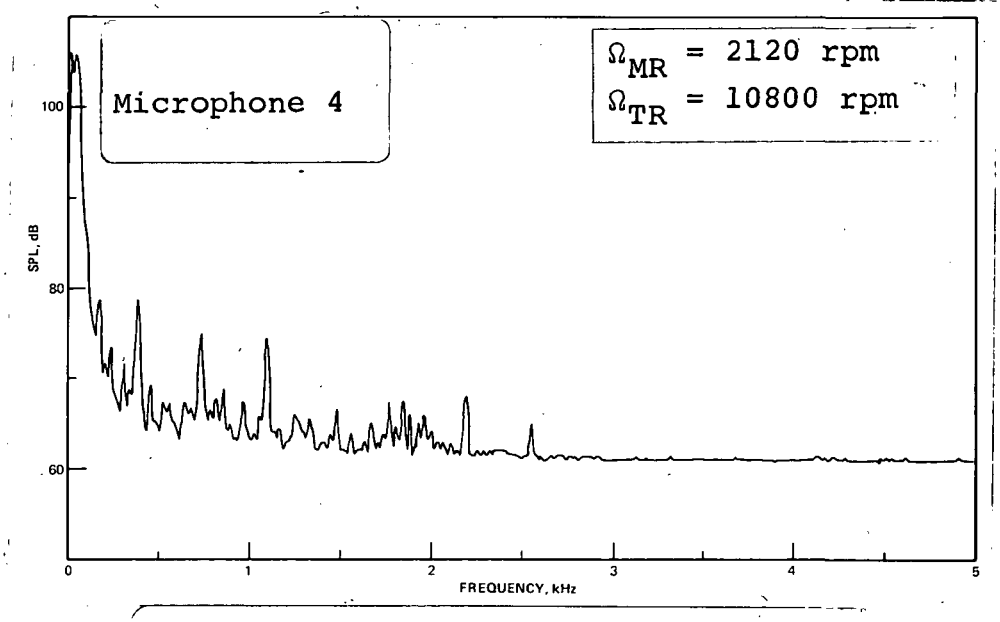

Figure 16. Measured Noise Spectrum of Configuration 3; μ = 0.28; Tail Rotor in Down Position

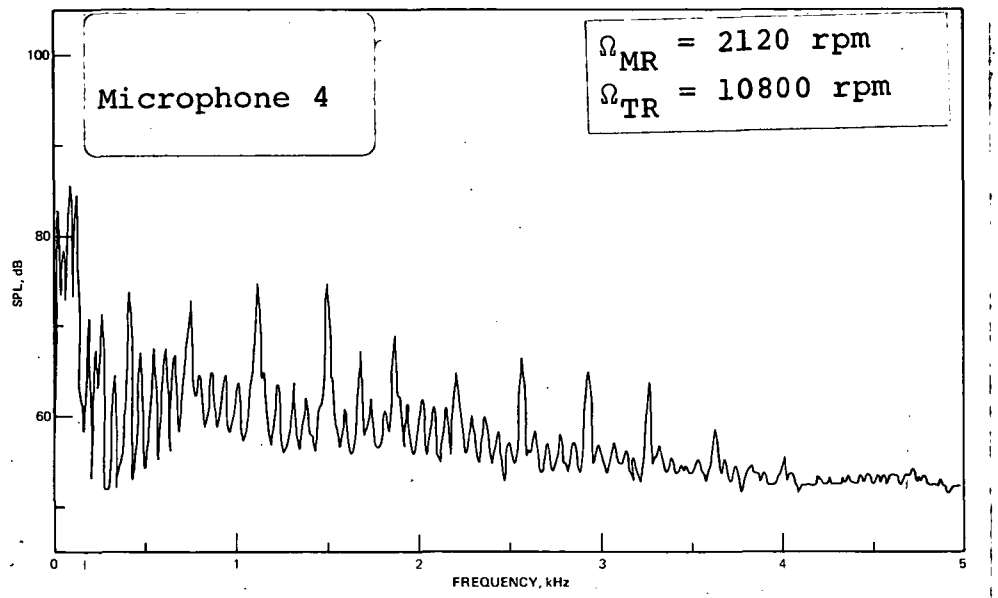

Figure 17. Measured Noise Spectrum of Configuration 4 in Hover

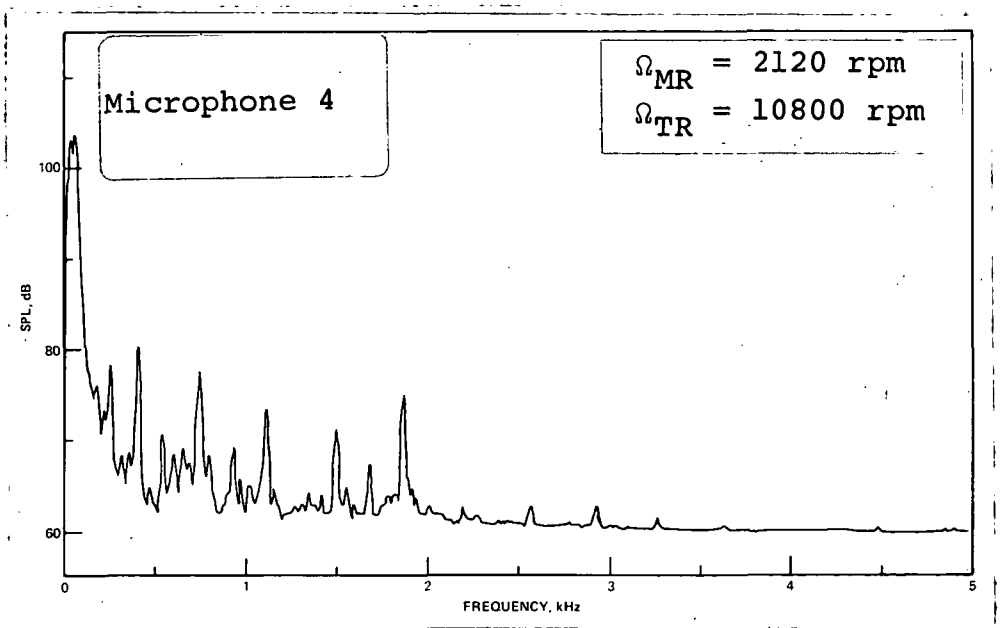

Figure 18. Measured Noise Spectrum of Configuration 4, μ = 0.20; Tail Rotor in Down Position

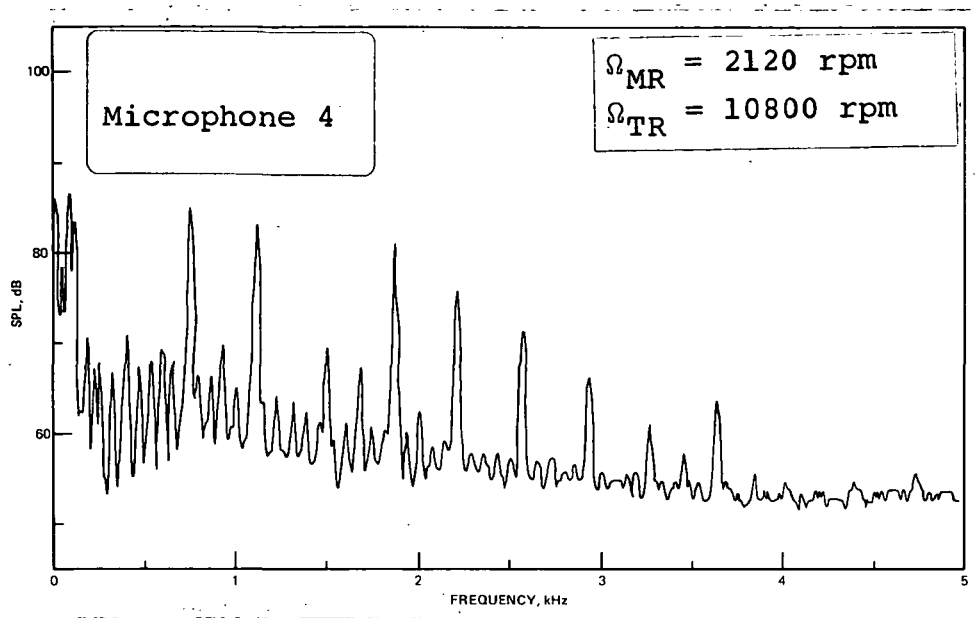

Figure 19. Measured Noise Spectrum of Configuration 5 in Hover

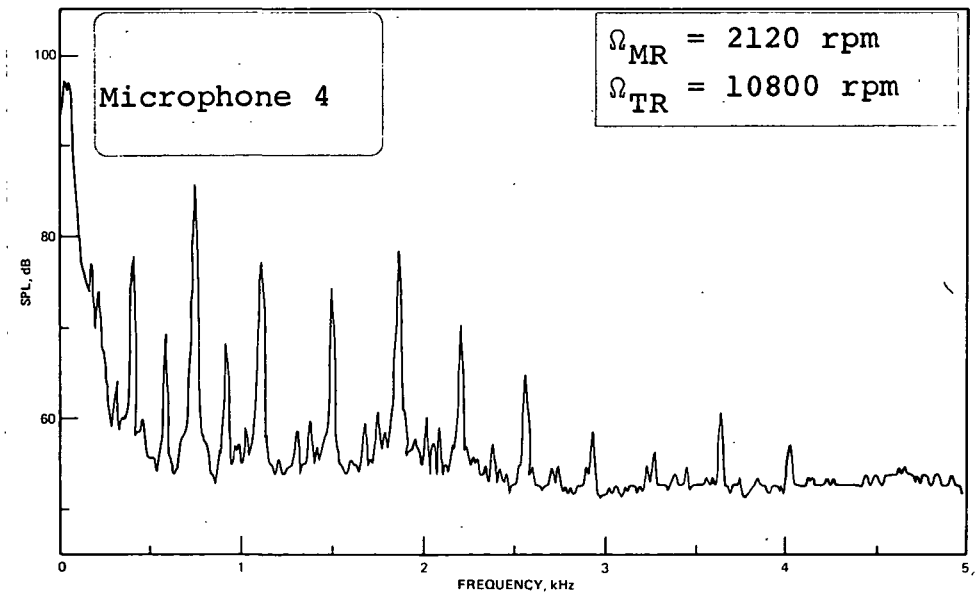

Figure 20. Measured Noise Spectrum of Configuration 5, μ = 0.09; Tail Rotor in Down Position

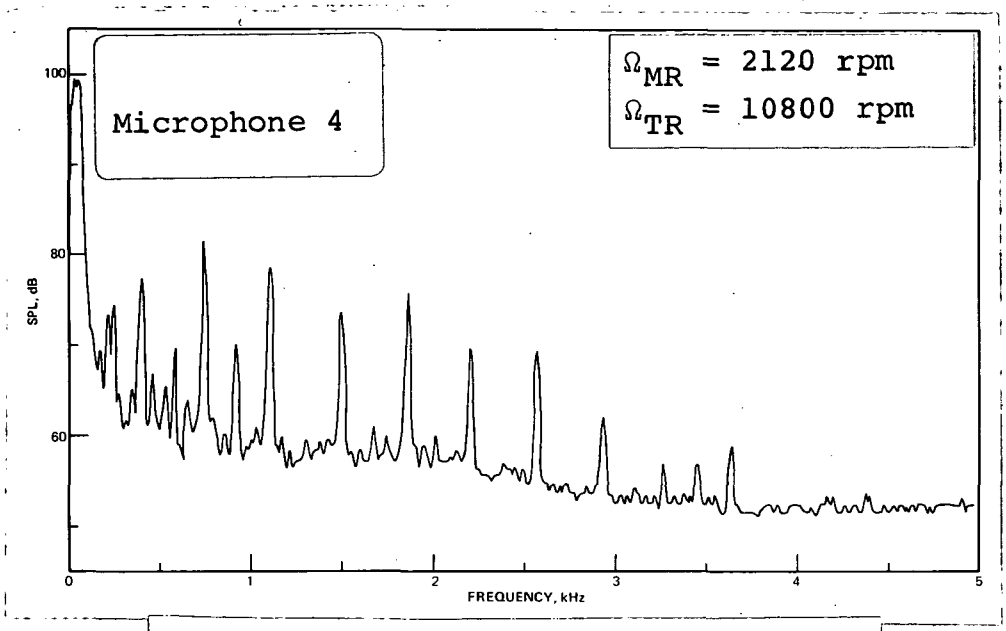

Figure 21. Measured Noise Spectrum of Configuration 5, μ = 0.20; Tail Rotor in Down Position

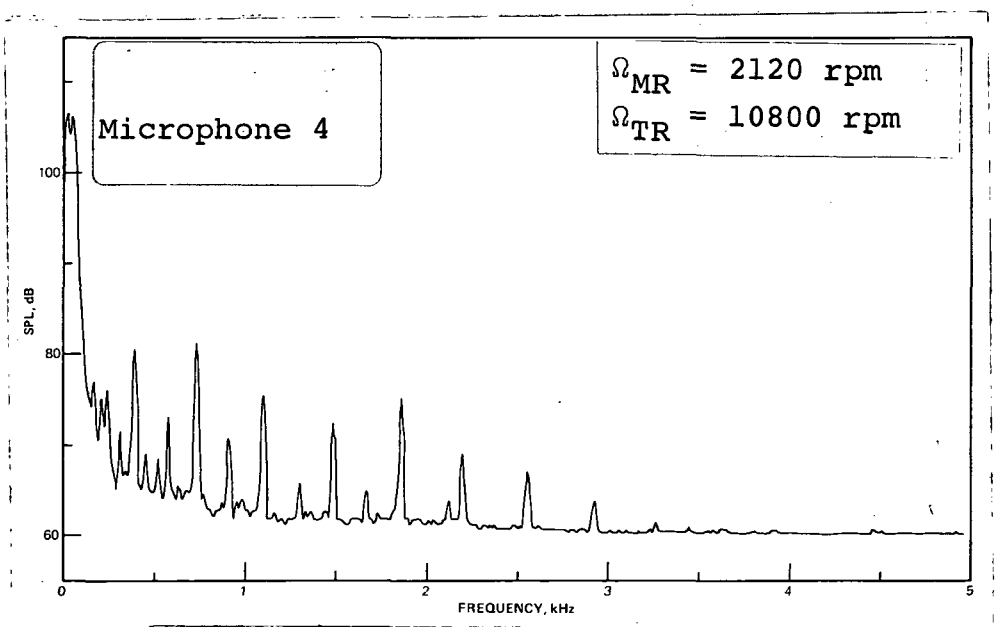

Figure 22. Measured Noise Spectrum of Configuration 5, μ = 0.28; Tail Rotor in Down Position

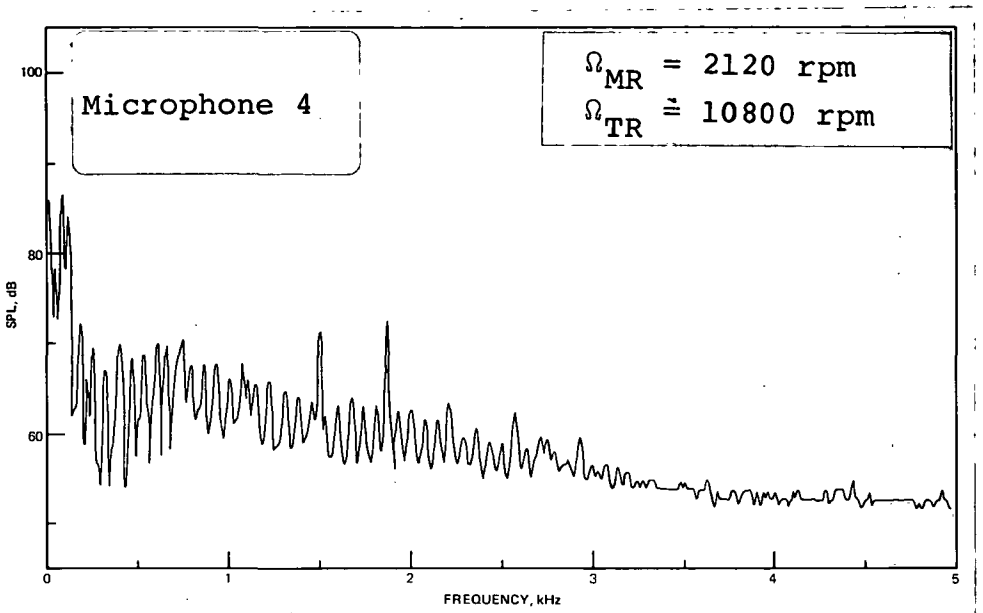

Figure 23. Measured Noise Spectrum of Configuration 6 in Hover

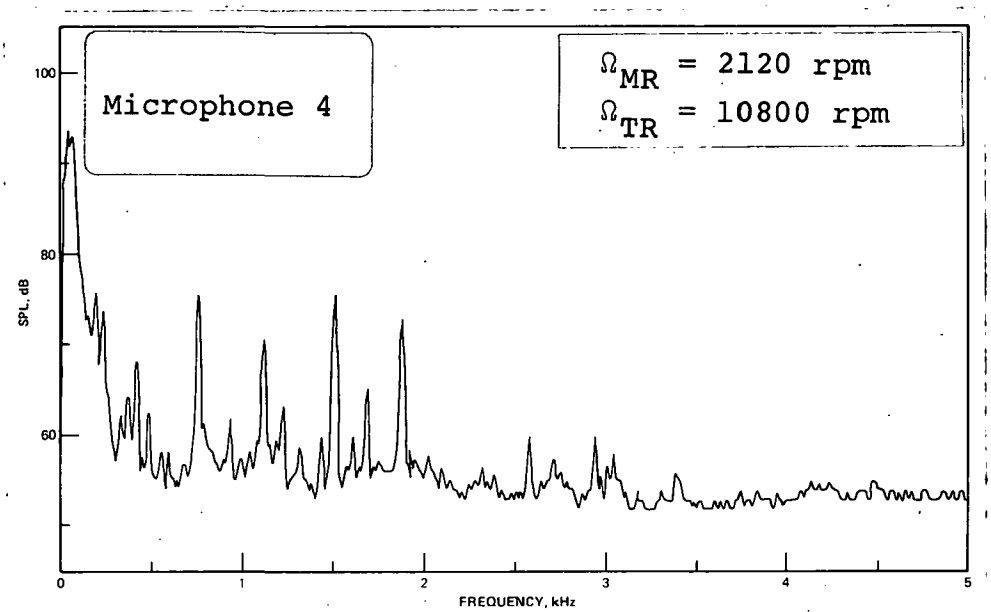

Figure 24. Measured Noise Spectrum of Configuration 6, μ = 0.09; Tail Rotor in Down Position

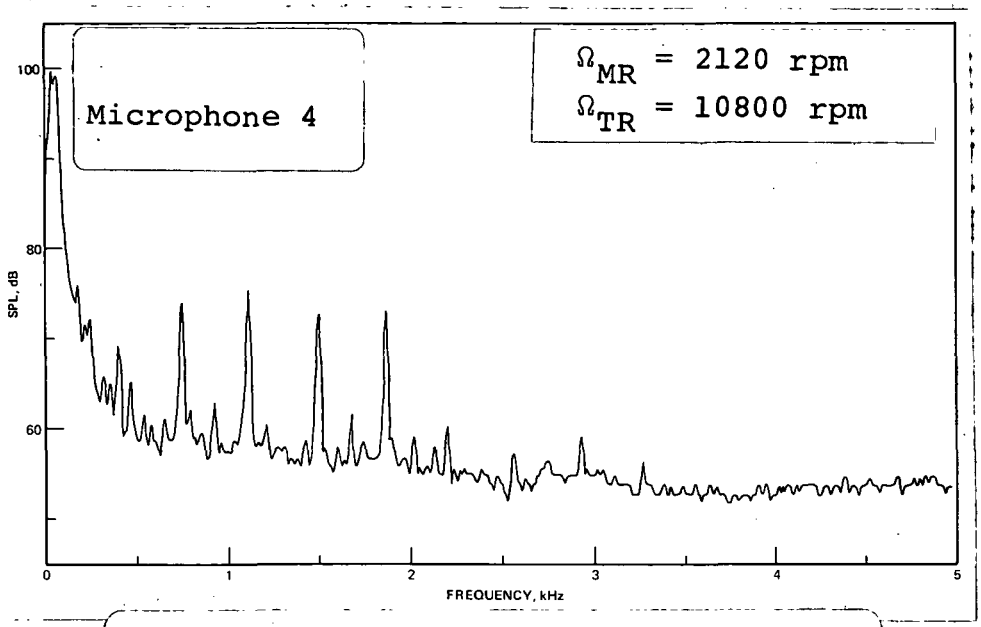

Figure 25. Measured Noise Spectrum of Configuration 6, μ = 0.20; Tail Rotor in Down Position

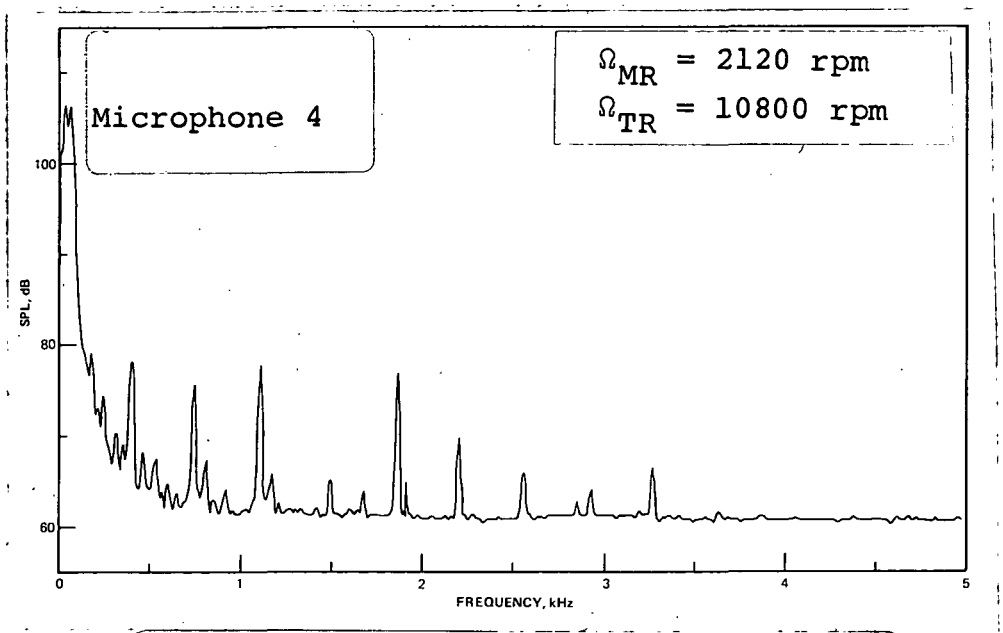

Figure 26. Measured Noise Spectrum of Configuration 6, μ = 0.28; Tail Rotor in Down Position

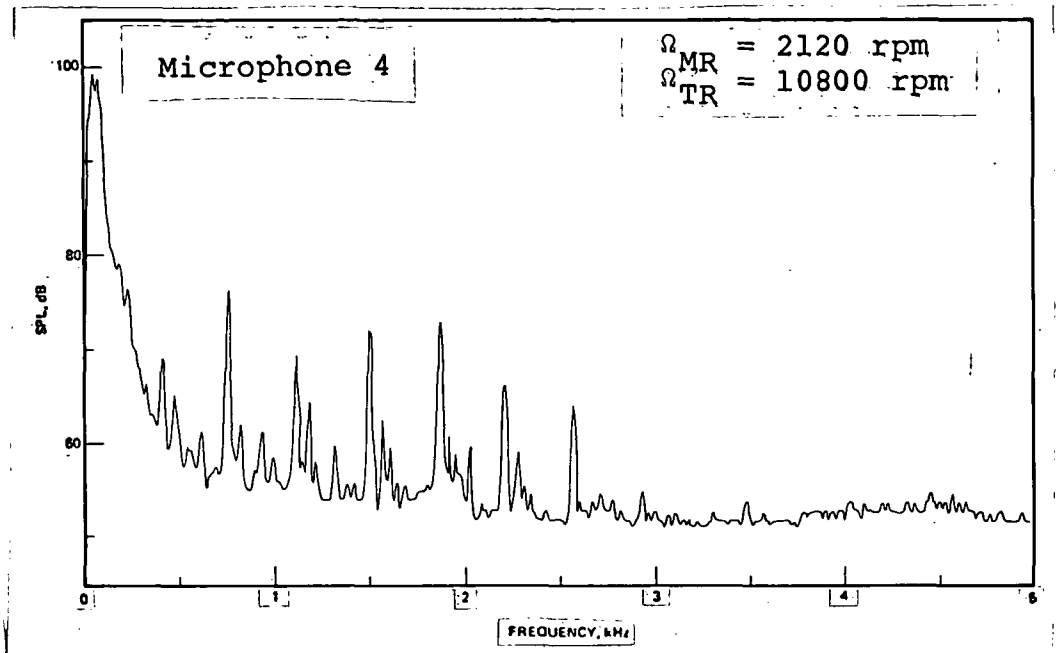

Figure 27. Measured Noise Spectrum of Configuration 6, μ = 0.09; Tail Rotor in Up Position

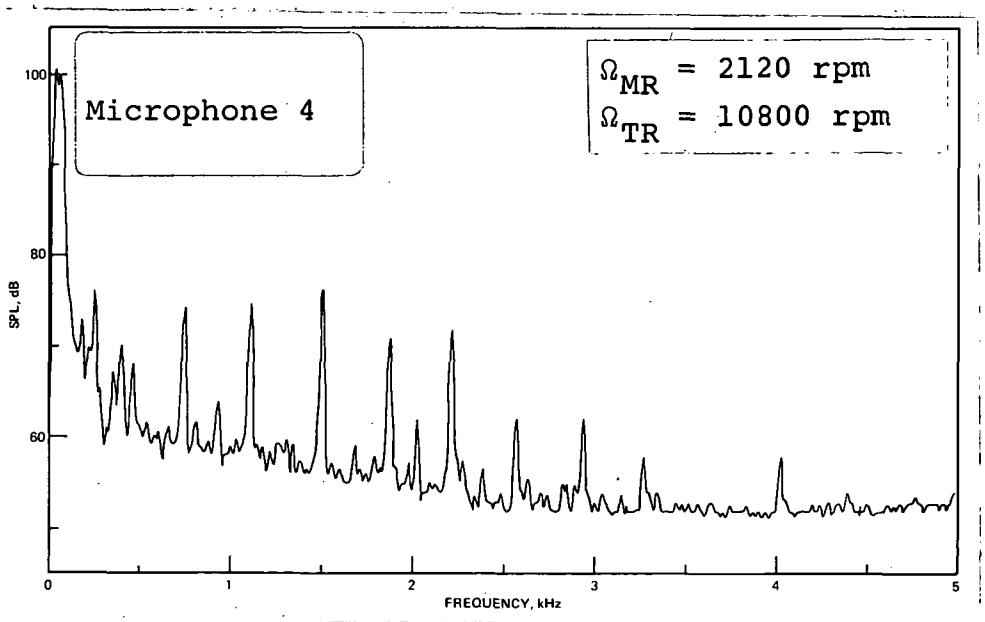

Figure 28. Measured Noise Spectrum of Configuration 6, μ = 0.20; Tail Rotor in Up Position

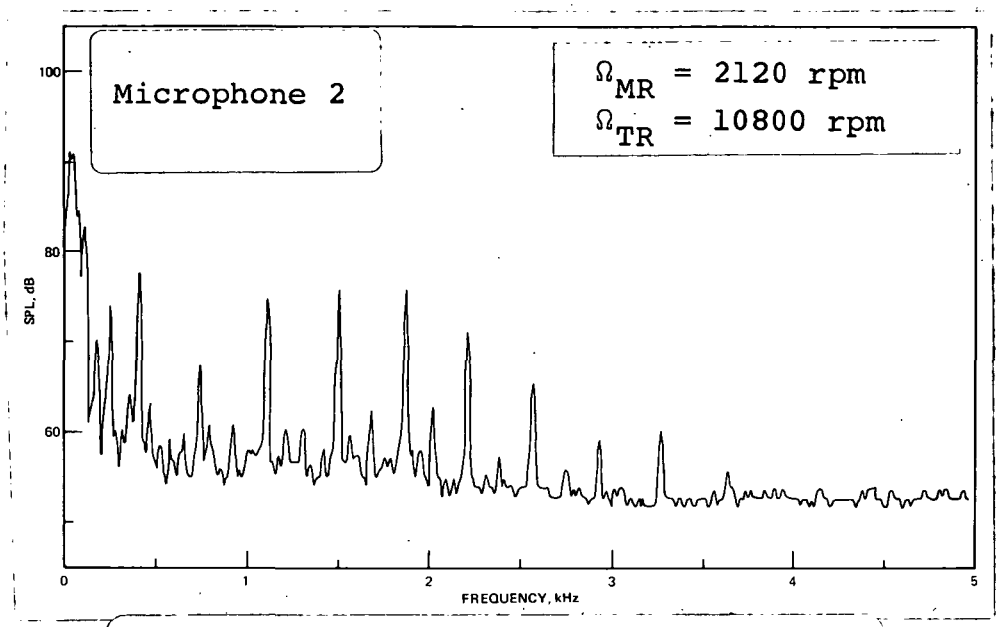

Figure 29. Measured Noise Spectrum of Configuration 6, μ = 0.20; Tail Rotor in Down Position

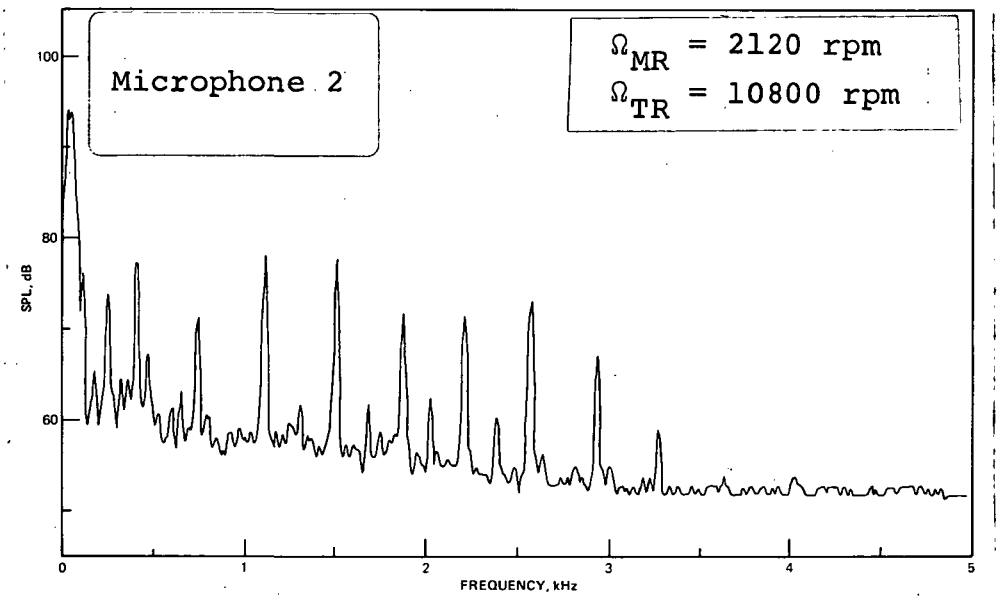

Figure 30. Measured Noise Spectrum of Configuration 6, μ = 0.20; Tail Rotor in Up Position

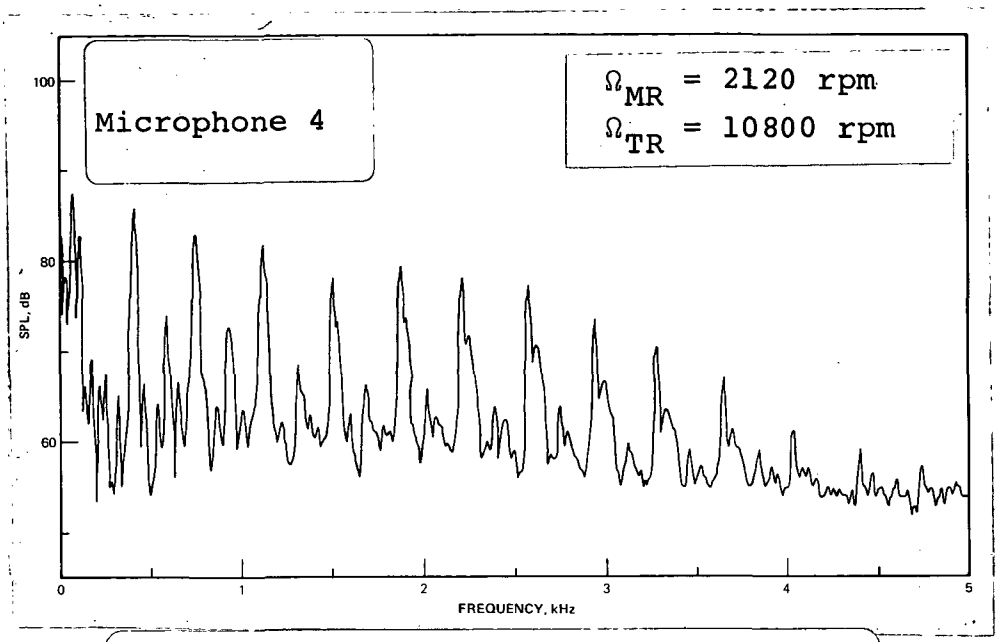

Figure 31. Measured Noise Spectrum of Configuration 7 in Hover

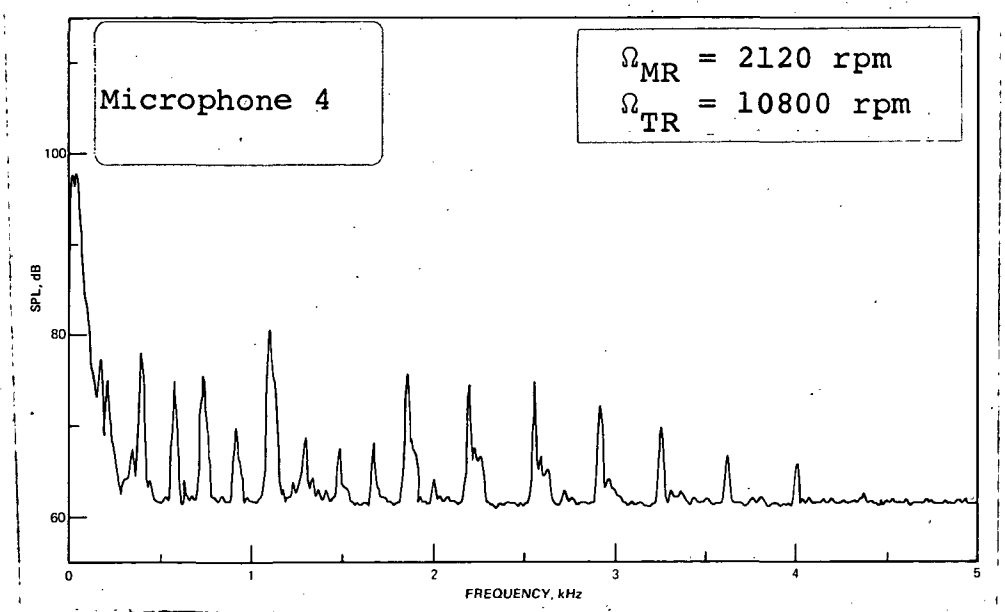

Figure 32. Measured Noise Spectrum of Configuration 7, μ = 0.09; Tail Rotor in Down Position

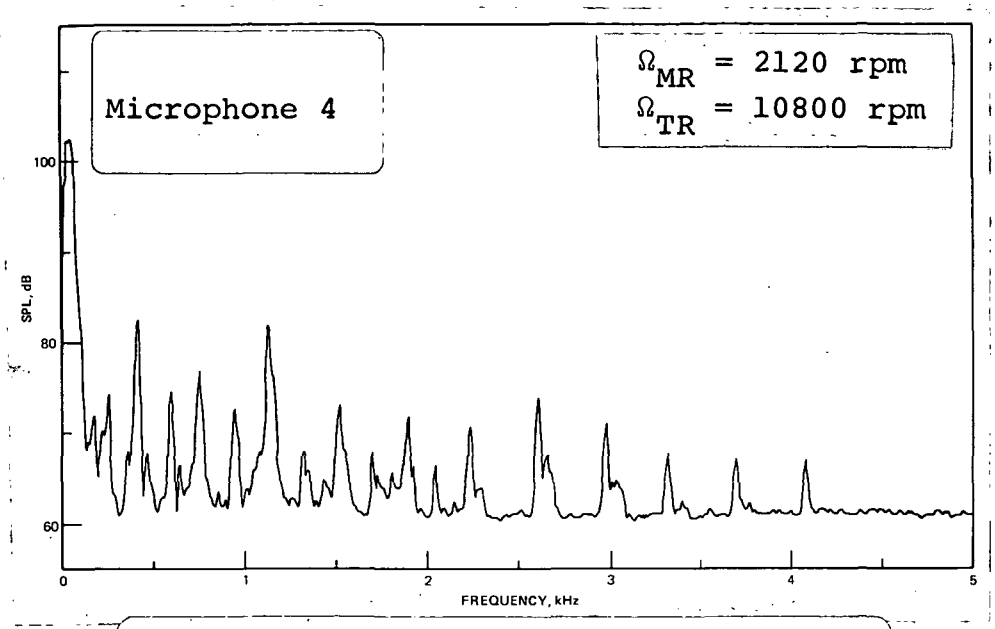

Figure 33. Measured Noise Spectrum of Configuration 7, μ = 0.20; Tail Rotor in Down Position

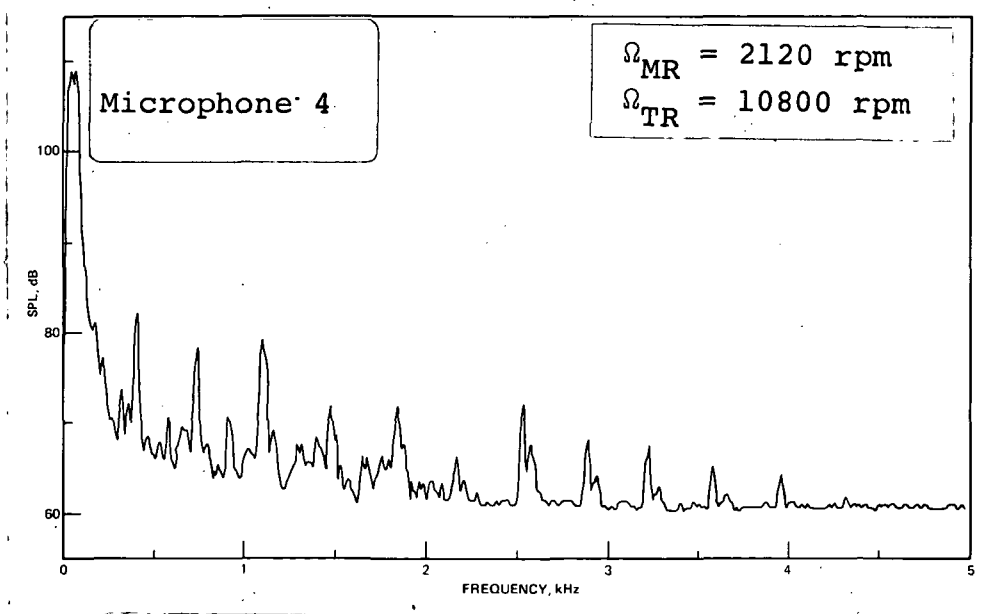

Figure 34. Measured Noise Spectrum of Configuration 7, μ = 0.28; Tail Rotor in Down Position

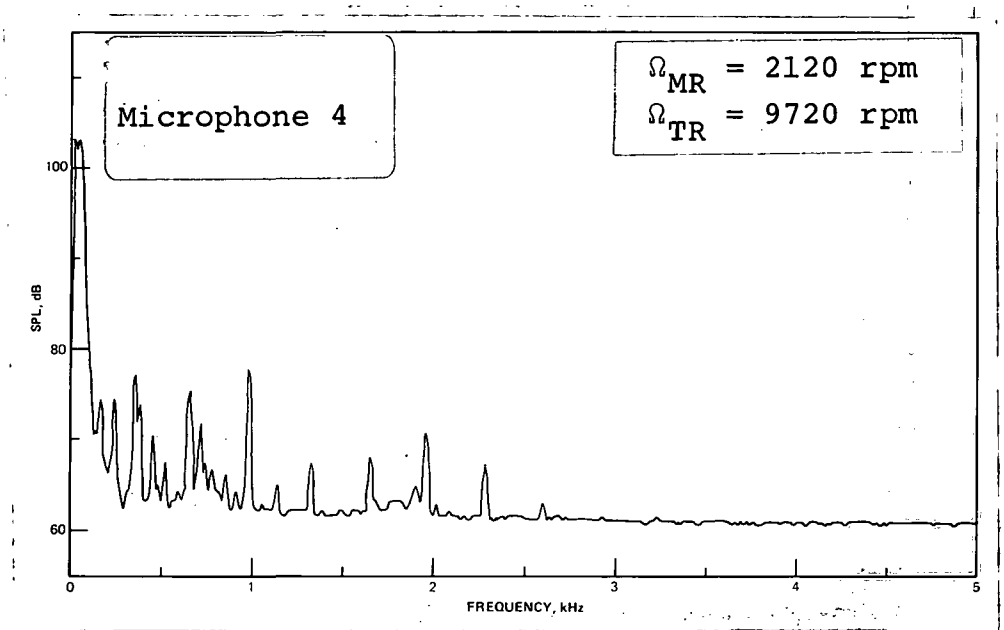

Figure 35. Measured Noise Spectrum of Configuration 8-1, μ = 0.20; Tail Rotor in Down Position

34

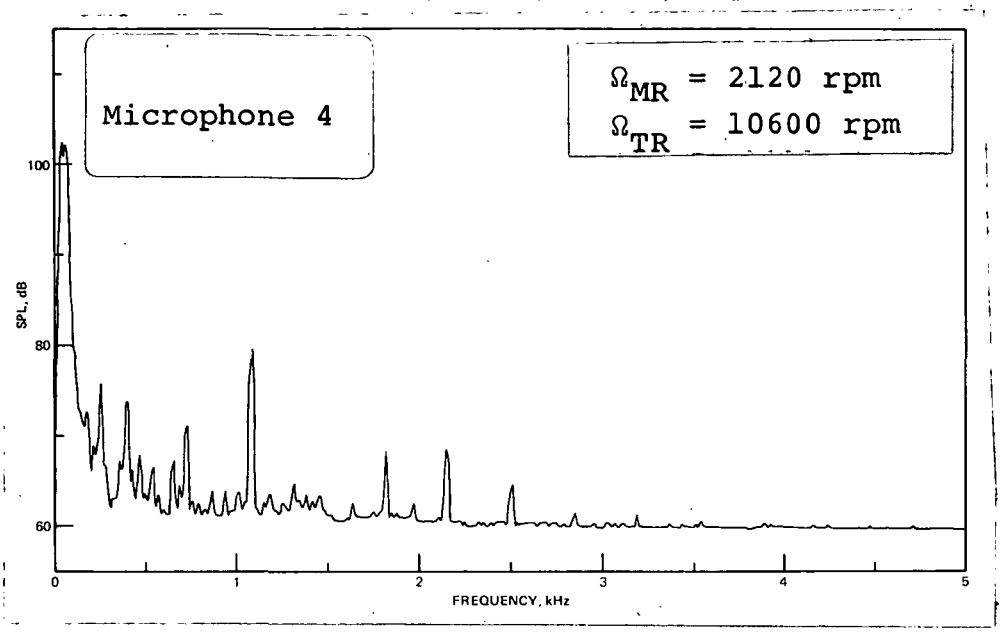

1.33-2

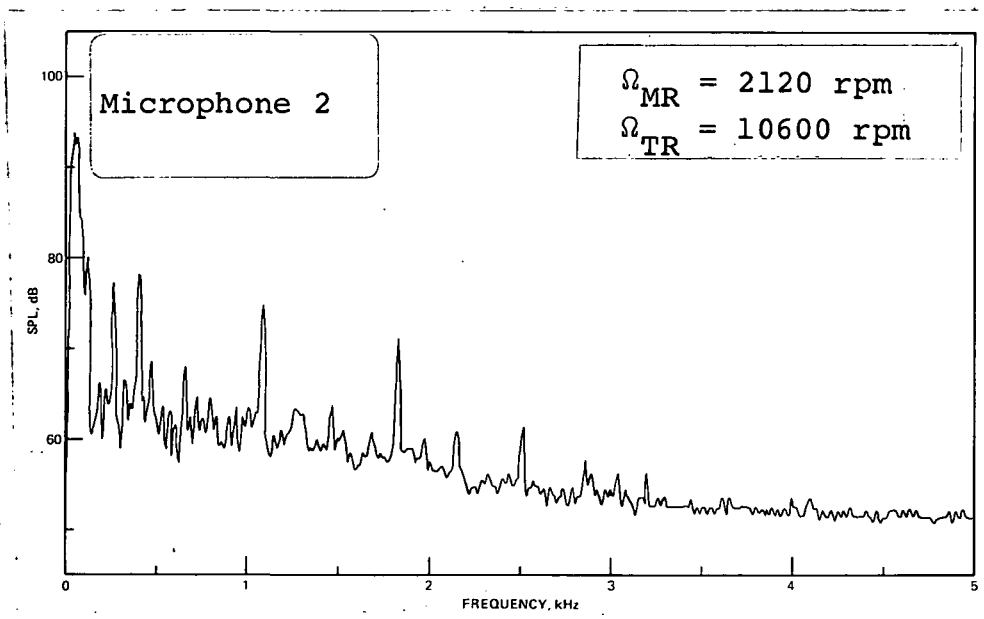

Figure 36. Measured Noise Spectrum of Configuration 8-2, μ = 0.20; Tail Rotor in Down Position

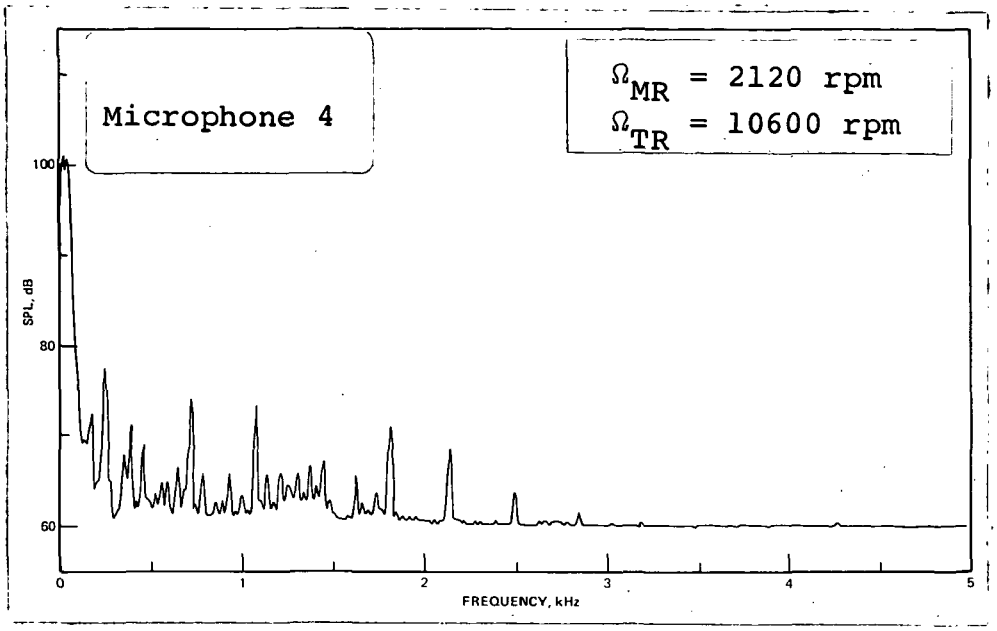

137-4

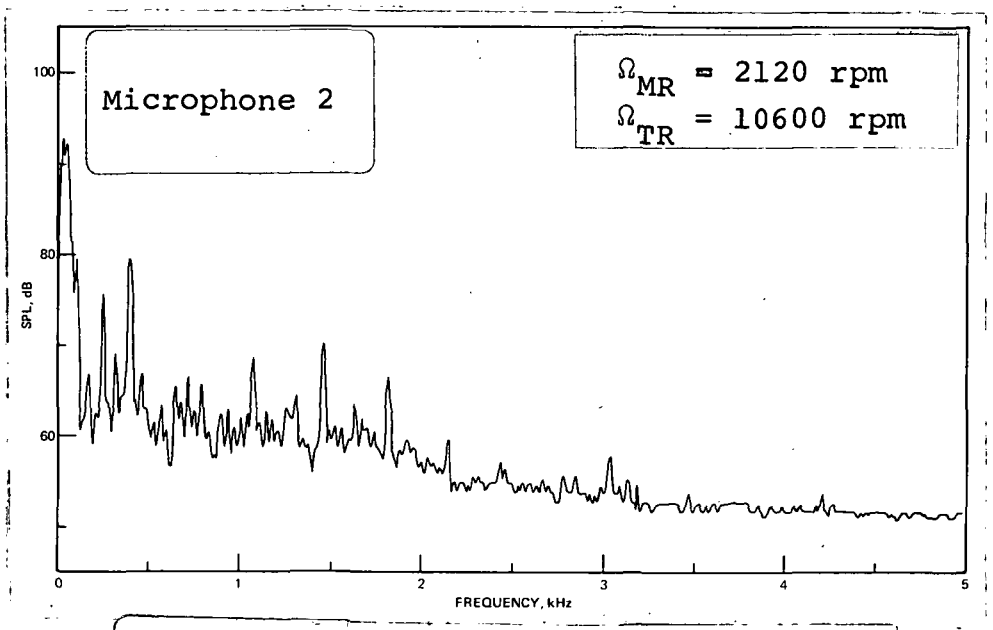

Figure 37. Measured Noise Spectrum of Configuration 8-2, μ = 0.20; Tail Rotor in Up Position.

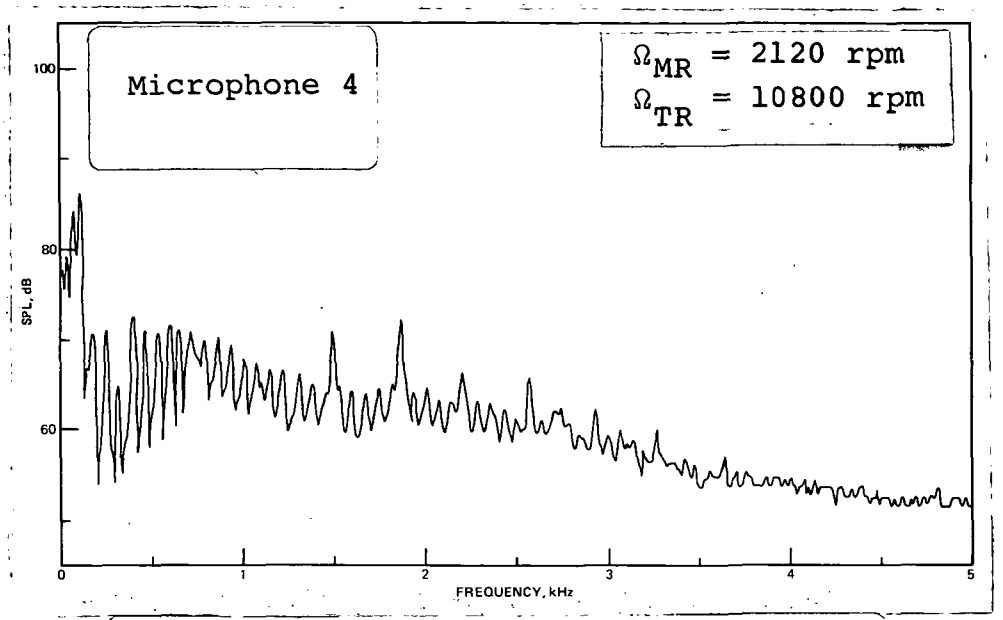

37

Figure 38. Measured Noise Spectrum of Configuration 9 in Hover

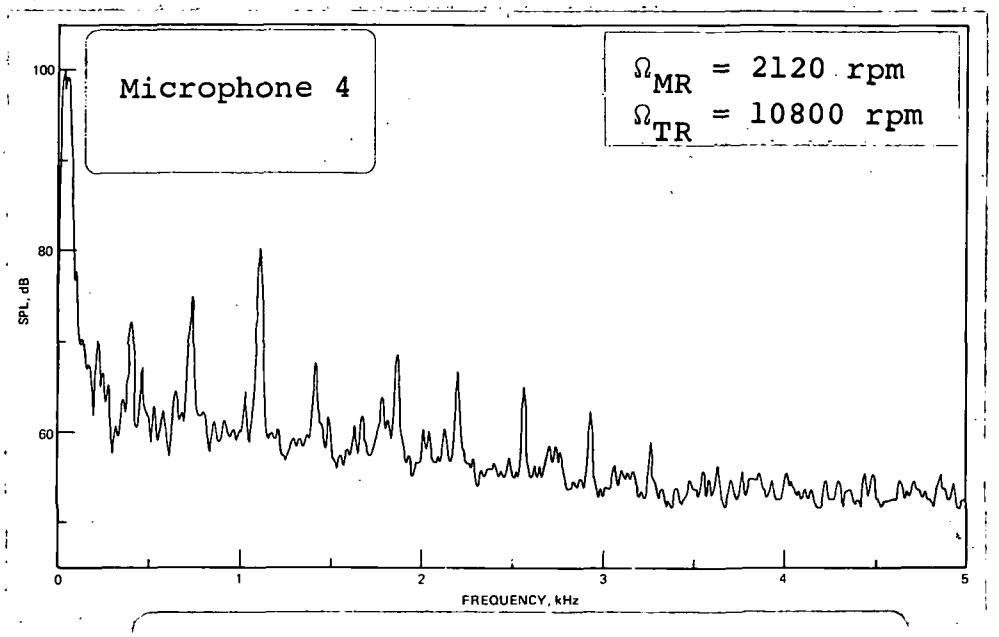

38

Figure 39. Measured Noise Spectrum of Configuration 9, μ = 0.20; Tail Rotor in Down Position

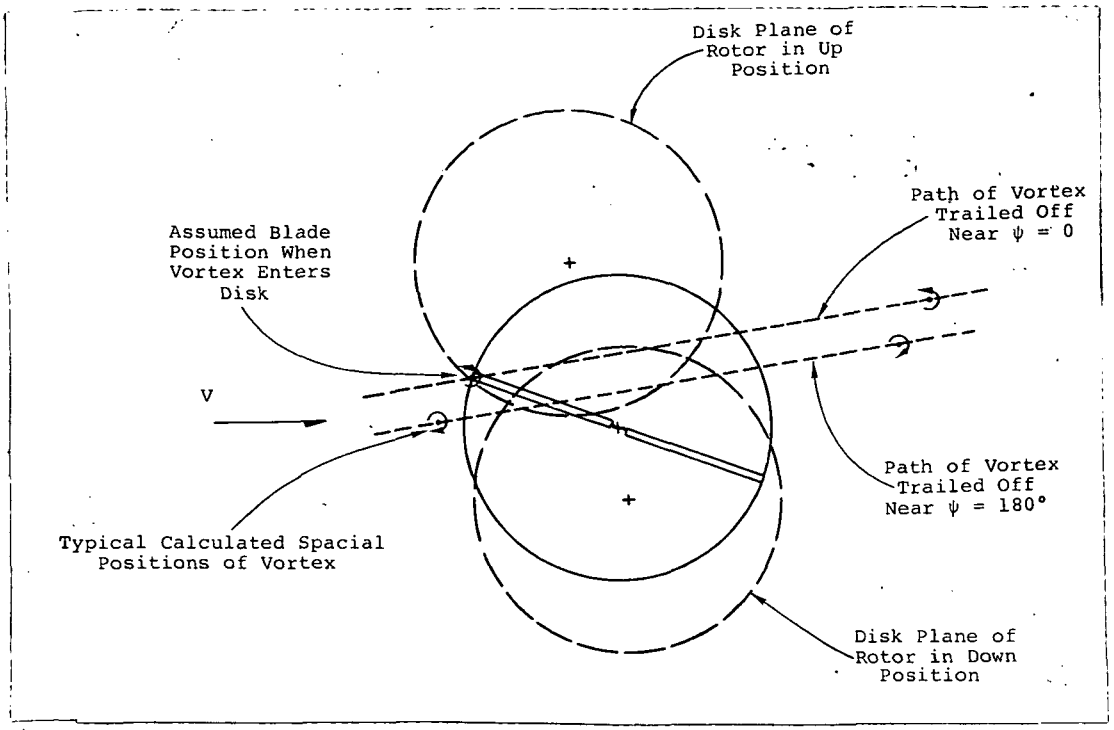

FIGURE 40. Main Rotor Wake/Tail Rotor Interaction Model; $\mu = 0.20$

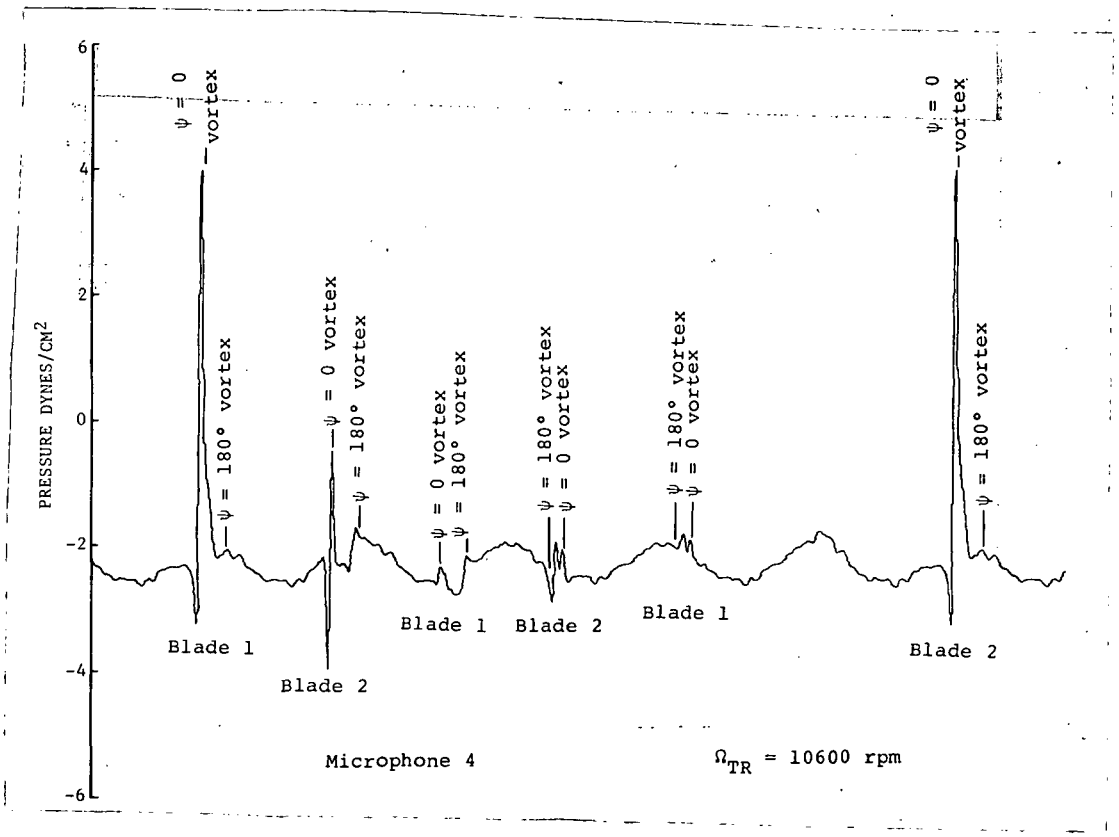

FIGURE 41. Calculated Sound Pressure vs Time with Periodic Main Rotor Wake Interaction, $\mu = 0.20$; Tail Rotor in Mid Position

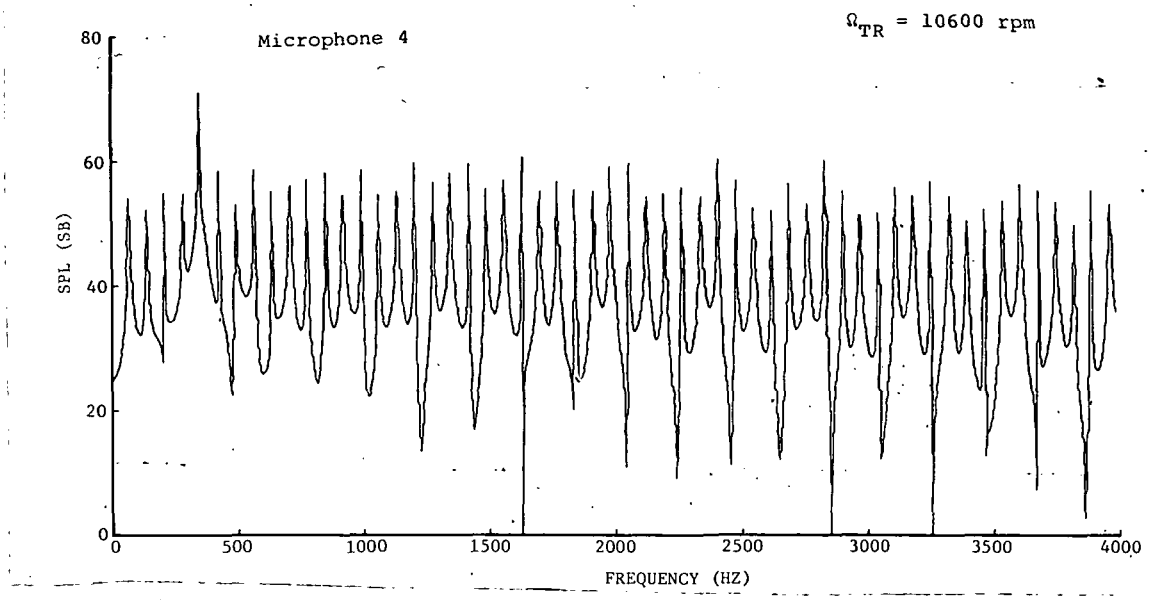

FIGURE 42. CALCULATED NOISE SPECTRUM WITH PERIODIC MAIN ROTOR WAKE INTERACTION, μ = 0.20; TAIL ROTOR IN MID POSITION

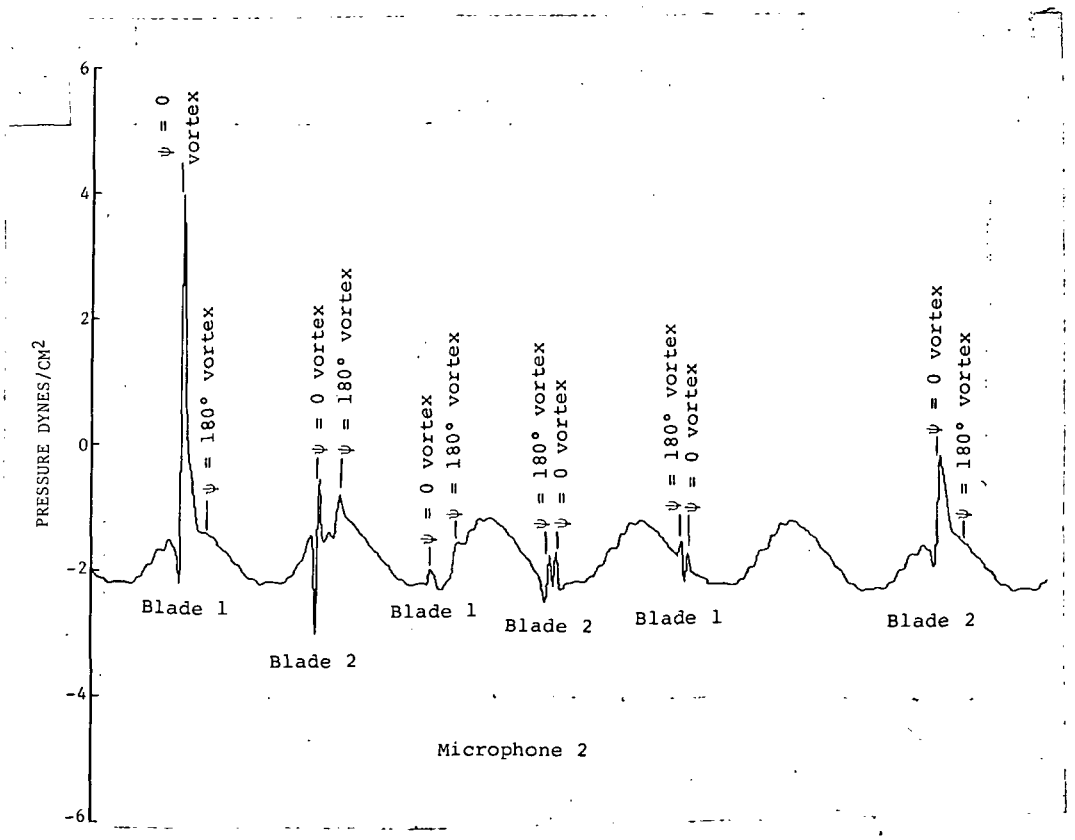

FIGURE 43. CALCULATED SOUND PRESSURE vs TIME WITH NONPERIODIC MAIN ROTOR WAKE INTERACTION; μ = 0.20; TAIL ROTOR IN MID POSITION

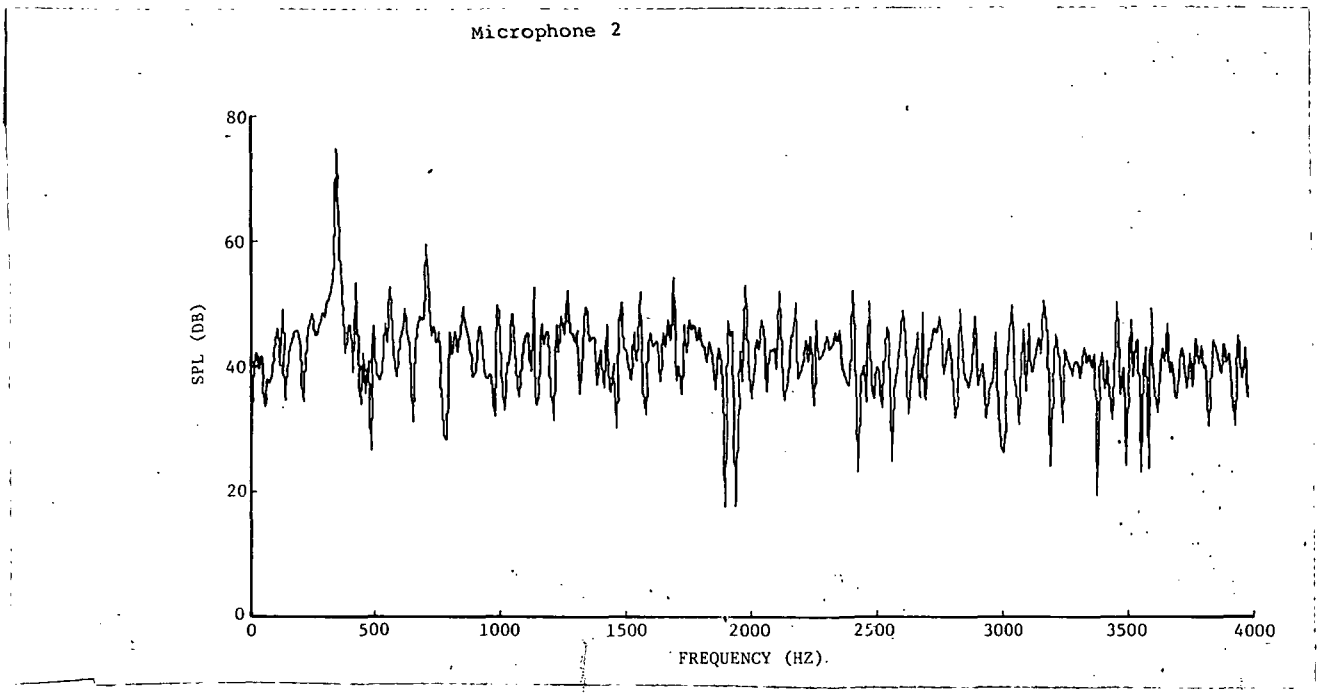

FIGURE 44. CALCULATED NOISE SPECTRUM WITH NONPERIODIC MAIN ROTOR WAKE INTERACTION; $\mu = 0.20$; TAIL ROTOR IN MID POSITION

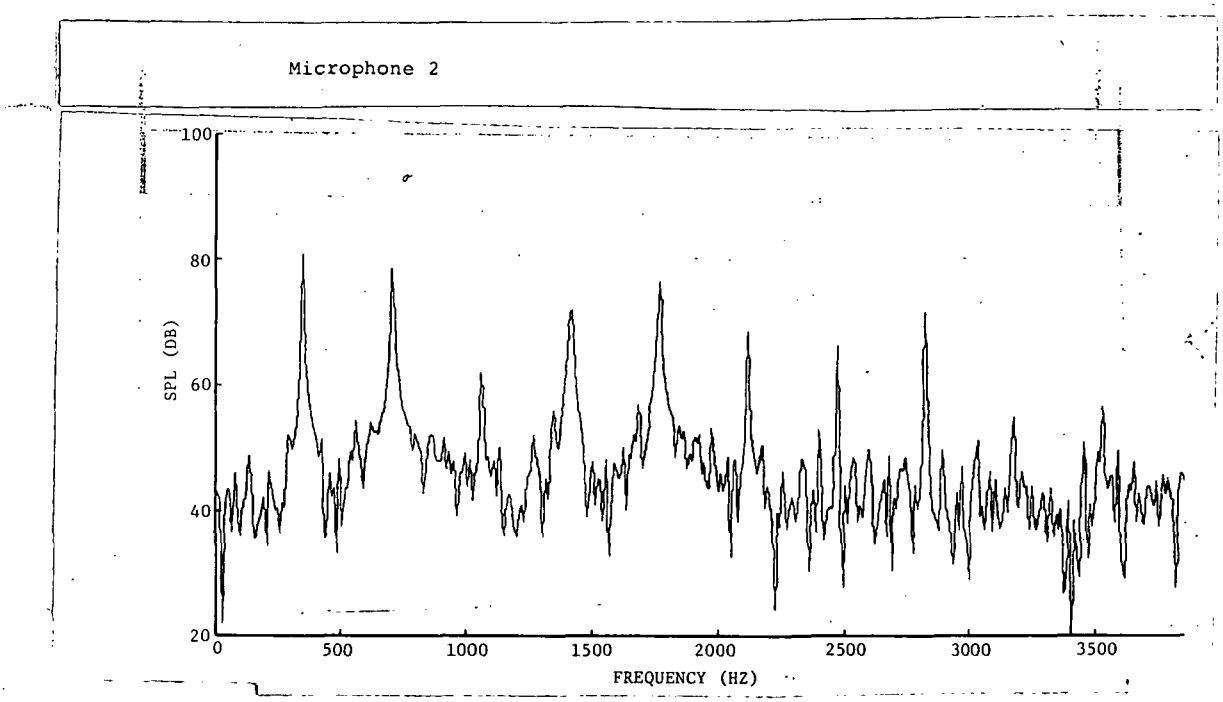

FIGURE 45. CALCULATED NOISE SPECTRUM WITH NONPERIODIC MAIN ROTOR WAKE INTERACTION AND NON-UNIFORM TAIL ROTOR WAKE; $\mu = 0.20$; TAIL ROTOR IN MID POSITION

APPENDIX A TYPICAL BACKGROUND NOISE MEASUREMENTS

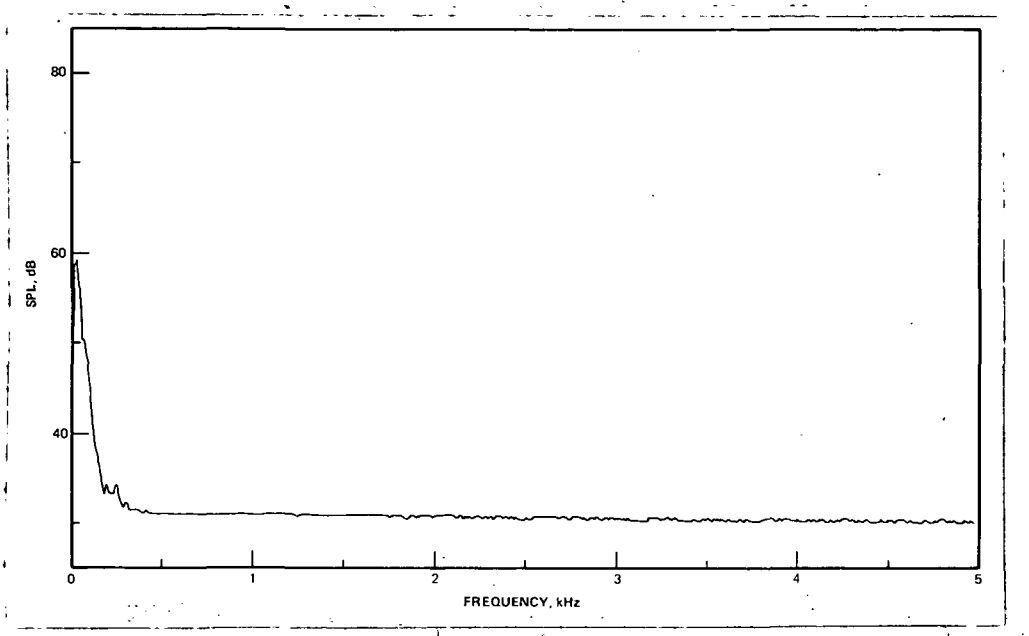

V = 0; Microphone 4

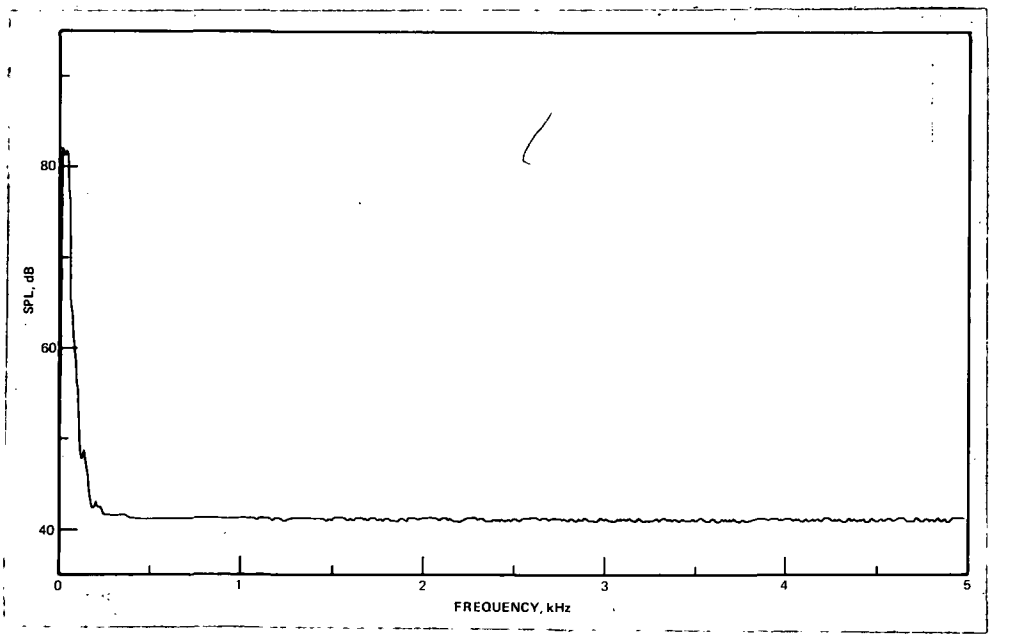

V = 9.1 m/sec; Microphone 4

APPENDIX A - Continued

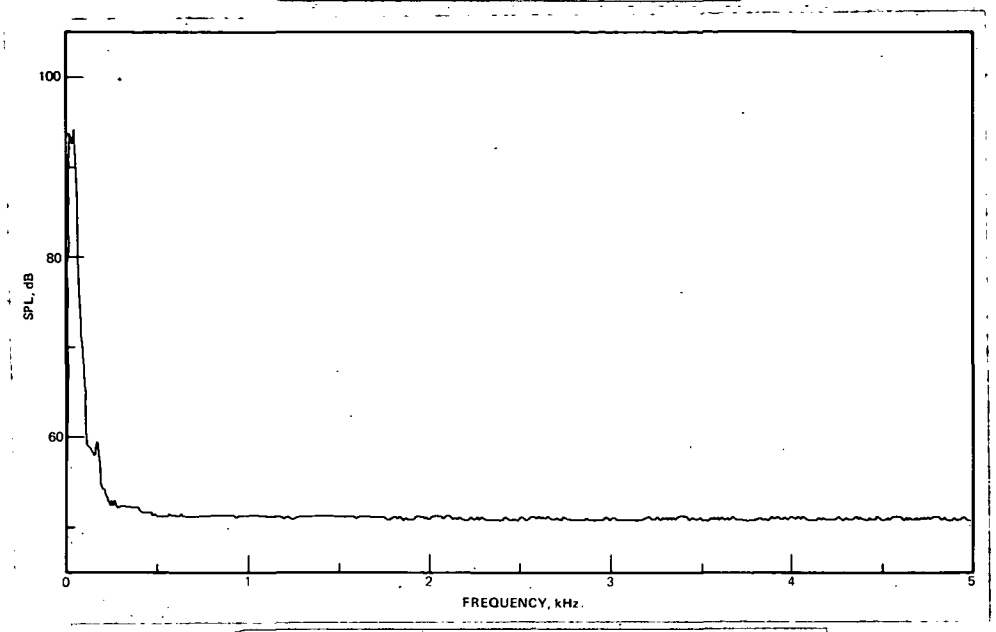

V = 20.1 m/sec; Microphone 4

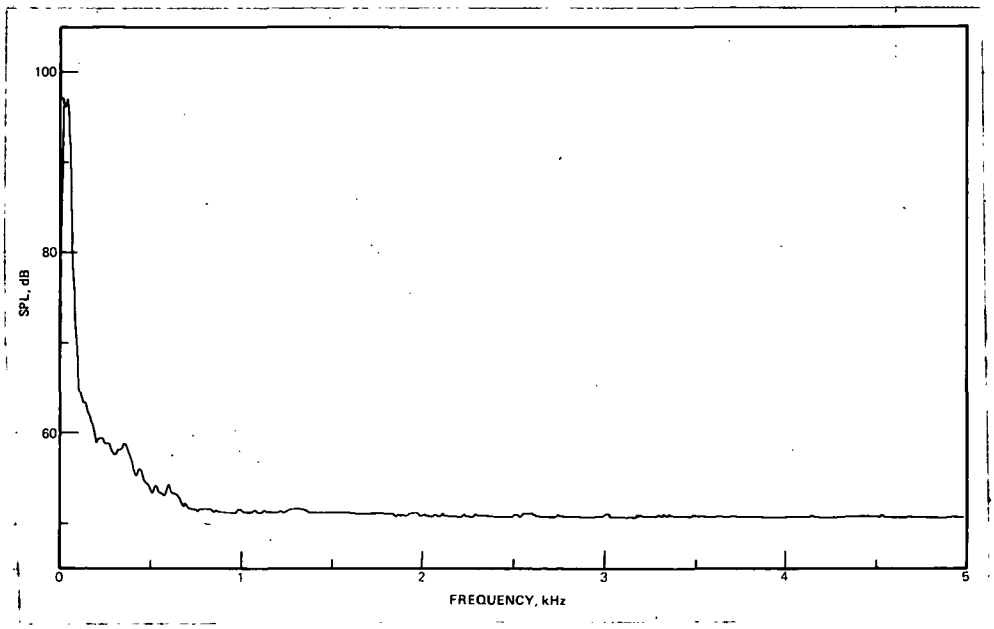

V = 28.4 m/sec; Microphone 4

APPENDIX B SUMMARY OF TEST CONDITIONS

Conf. No.	V m/sec	Main Rotor RPM	Main Rotor α_s, deg	Main Rotor θ_0, deg	Tail Rotor RPM	Tail Rotor θ_0, deg	Tail Rotor α_z, deg	Rec. No.
1	0	0	0	11.5	10800	7.0	-19.6	16
				14.0		6.0	-19.6	60
			-6	12.0		4.0	-19.6	96
		2120	0	11.5	0	7.0	-19.6	14
				14.0		6.0	-19.6	58
				11.5	10800	7.0	-19.6	15
				14.0		6.0	-19.6	59
	9.1		-3	11.5		5.0	-19.6	21
							-10.8	22
				12.0		4.0	-19.6	74
							-10.8	75
							- 6.4	76
							- 1.8	77
					10880		+ 2.1	186
	20.1		-6	11.5	10800	5.0	-10.8	17
							-19.6	18
				12.0		4.0	-19.6	78
							-10.8	79
							- 6.4	80
					10880		+ 2.1	188
	28.4		-10	11.5	10800	5.0	-19.6	19
							-10.8	20
				14.0		4.0	-19.6	55
							-10.8	56
							- 6.4	57
					10880		+ 2.1	189
2	9.1	2120	-3	11.5	10800	4.0	-19.6	23
							-10.8	24
				12.0		3.0	-19.6	84
							-10.8	85
							- 6.4	86
	20.1		-6	11.5		4.0	-19.6	25
							-14.1	26
				12.0		3.0	-19.6	81
							-10.8	82
							- 6.4	83
	28.4		-10	11.5	0	4.0	-14.1	27
				14.0	10800	3.0	-19.6	87
							-10.8	89
3	9.1	2120	-3	12.0	10800	4.0	-10.8	117
							+ 2.1	118
							-19.6	119
	20.1		-6				-19.6	114
							+ 2.1	115

APPENDIX B Continued

Conf. No.	V m/sec	Main Rotor RPM	Main Rotor α_s, deg	Main Rotor θ_0, deg	Tail Rotor RPM	Tail Rotor θ_0, deg	Tail Rotor α_z, deg	Rec. No.
3	20.1	2120	-6	12.0	10800	4.0	-10.8	116
	28.4		-10	14.0			-19.6	110
							+ 2.1	111
							-10.8	112
							-14.1	113
4	0	2120	0	14.0	10800	6.0	-19.6	61
		0					-19.6	62
	9.1	2120	-3	12.0		4.0	-19.6	69
							-10.8	70
							-10.8	71
							- 6.4	72
							- 1.8	73
	20.1		-6				-19.6	66
							-10.8	67
							- 6.4	68
	28.4		-10	14.0			-19.6	63
							-10.8	64
							- 6.4	65
5	0	2120	0	14.0	10880	6.0	-10.8	170
	9.1		-3	12.0		4.0	-19.6	177
							+ 2.1	178
							-10.8	179
	20.1		-6				-10.8	174
							+ 2.1	175
							-19.6	176
	28.4		-10	14.0			-10.8	171
							+ 2.1	172
							-19.6	173
6	0	2120	0	14.0	10880	6.0	-10.8	169
	9.1		-3	12.0		4.0	-19.6	163
							-10.8	164
							+ 2.1	165
	20.1		-6				-10.8	160
							+ 2.1	161
							-19.6	162
	28.4		-10	14.0			-10.8	166
							+ 2.1	167
							-19.6	168
7*	0	0	0	14.0	10800	2.0	-10.8	128
		2120			10900		-10.8	127
	9.1		-3	12.0	10880		-19.6	121
					10850		+10.2	122
					10800		-10.8	123

APPENDIX B Continued

Conf. No.	V m/sec	Main Rotor RPM	Main Rotor α_s, deg	Main Rotor θ_0, deg	Tail Rotor RPM	Tail Rotor θ_0, deg	Tail Rotor α_z, deg	Rec. No.
7*	20.1	2120	-6	12.0	10800	2.0	-10.8	124
							+10.2	125
					11000		-19.6	126
	28.4		-10	14.0	10870		-10.8	129
							+10.2	130
							-19.6	131
8-1	0	2120	0	14.0	9720	4.6	-10.8	104
		0					-10.8	105
	9.1	2120	-3	12.0			-19.6	97
							-19.6	98
							-14.1	99
							- 1.8	100
	20.1		-6				- 1.8	101
							-10.8	102
							-19.6	103
	28.4		-10	14.0			-19.6	106
							-10.8	107
							- 1.8	108
							+ 2.1	109
8-2	0	2123	0	14.0	10600	5.9	-10.8	132
	9.1	2120	-3	12.0	10600	4.0	-19.6	139
							+ 2.1	140
							-10.8	141
	20.1		-6				-10.8	136
							+ 2.1	137
							-19.6	138
	28.4		-10	14.0			-19.6	133
							+ 2.1	134
							-10.8	135
9	0	2120	0	16.0	10870	7.0	-10.8	148
		0					-10.8	149
	9.1	2120	-3	14.0	10890	5.0	-10.8	142
							+ 2.1	143
							-19.6	144
	20.1		-6		10870		-19.6	145
							+ 2.1	146
							-10.8	147
	28.4		-10	16.0	10880		-10.8	156
							+ 2.1	157
							-19.6	158
P	36.6	2550	-10	12.0	13000	2.5	-10.8	159

* The tail boom is in an extended position because of the larger diameter tail rotor, although the spacing between the main and tail rotor planes is the same as the Reference Configuration.

APPENDIX C - MEASURED OVERALL NOISE LEVELS

Record Number	Measured Overall Noise Level (dB) for Microphone No.					
	1	2	3	4	5	6
1-55		Data Not Recorded				
55	117	108	120	115	114	116
56	116	108	122	122	114	117
57	115	110	123	122	116	118
58	108	109	110	108	109	106
59	109	110	110	109	110	108
60	94	95	98	99	99	94
61	108	109	110	109	109	108
62	94	95	97	100	99	95
63	113	108	120	118	114	116
64	114	107	119	118	114	116
65	114	118	120	118	113	117
66	111	115	115	113	119	113
67	110	113	116	112	118	113
68	110	114	115	115	118	113
69	109	111	112	110	113	109
70	109	111	115	112	113	109
71	109	111	111	108	112	109
72	109	111	112	111	111	109
73	109	111	115	110	112	109
74	109	111	112	120	122	109
75	109	111	114	121	121	109
76	109	111	114	122	112	109
77	109	110	114	120	111	109
78	113	115	116	113	120	115
79	114	116	119	116	120	115
80	114	114	117	114	118	115
81	113	114	116	114	119	115
82	113	114	118	115	115	114
83	112	115	118	117	121	115
84	109	110	112	111	124	109
85	108	111	114	110	113	109
86	109	110	114	111	111	109
87	114	116	120	117	114	116
88		Data Not Recorded				
89	114	118	120	117	113	116
90-95		Microphone Calibrations				
96	95	98	99	101	99	95
97	109	110	115	110	104	101
98	109	111	109	113	114	111
99	109	112	110	107	114	111
100	109	110	112	108	112	111
101	114	114	118	112	111	116

APPENDIX C Continued

Record Number	Measured Overall Noise Level (dB) for Microphone No.					
	1	2	3	4	5	6
102	113	115	117	114	120	115
103	112	114	116	110	119	115
104	109	111	111	110	110	111
105	94	94	97	99	98	92
106	105	119	121	118	114	117
107	105	119	120	120	113	117
108	113	118	119	116	114	117
109	114	117	120	119	115	117
110	114	117	118	117	123	117
111	114	119	120	118	122	116
112	114	119	120	119	113	117
113	114	107	120	120	114	117
114	113	115	115	112	117	116
115	113	114	115	112	119	115
116	113	114	114	111	119	116
117	109	110	109	116	121	111
118	109	111	110	115	121	111
119	110	111	112	120	112	111
120	Data Not Recorded					
121	109	111	112	109	110	111
122	110	111	110	107	109	111
123	110	110	113	112	111	111
124	114	114	116	112	110	116
125	115	116	117	111	109	117
126	113	115	117	113	109	116
127	110	111	112	113	112	109
128	100	103	106	109	108	100
129	115	117	123	120	112	118
130	115	117	123	120	111	116
131	115	120	122	116	113	117
132	110	110	111	110	111	110
133	115	118	122	122	114	117
134	113	118	121	120	111	117
135	114	117	122	121	114	116
136	113	114	114	112	108	116
137	112	114	115	112	108	115
138	114	114	115	112	109	116
139	110	110	109	106	114	111
140	110	111	110	117	121	111
141	110	110	110	117	122	110
142	109	110	111	121	121	111
143	111	110	118	122	120	111
144	110	110	110	110	119	111
145	110	113	113	119	122	114
146	110	112	112	119	121	114
147	111	113	113	118	121	114
148	111	111	111	110	111	110
149	95	97	97	98	98	94

Record Number	Measured Overall Noise Level (dB) for Microphone No.					
	1	2	3	4	5	6
150-155		Microphone Calibrations				
156	114	118	120	118	122	118
157	114	117	120	119	123	117
158	113	118	120	119	123	118
159	120	124	123	123	124	121
160	112	112	116	124	115	116
161	114	114	114	120	115	116
162	110	111	115	124	117	116
163	110	111	108	115	124	110
164	110	109	111	120	124	109
165	110	110	112	119	115	110
166	114	119	119	115	122	116
167	113	120	120	117	122	115
168	114	118	117	117	121	116
169	110	111	111	109	110	108
170	110	110	111	111	111	108
171	112	117	116	116	121	116
172	114	118	117	113	120	116
173	115	119	117	119	122	117
174	115	116	118	120	117	116
175	114	114	115	118	117	114
176	113	115	121	120	117	114
177	110	110	110	115	114	108
178	110	109	111	115	113	108
179	109	109	111	118	112	108
180-185		Microphone Calibrations				
186	109	109	108	120	110	109
187-188		Data Not Recorded				
189	112	119	116	119	120	117